A&A 619, A32 (2018)
https://doi.org/10.1051/0004-6361/201833440

Astronomy & Astrophysics

The CARMENES search for exoplanets around M dwarfs

Nine new double-line spectroscopic binary stars

D. Baroch[1,2], J. C. Morales[1,2], I. Ribas[1,2], L. Tal-Or[3,4], M. Zechmeister[3], A. Reiners[3], J. A. Caballero[5], A. Quirrenbach[6], P. J. Amado[7], S. Dreizler[3], S. Lalitha[3], S. V. Jeffers[3], M. Lafarga[1,2], V. J. S. Béjar[8,9], J. Colomé[1,2], M. Cortés-Contreras[7,5], E. Díez-Alonso[5], D. Galadí-Enríquez[10], E. W. Guenther[11], H.-J. Hagen[12], T. Henning[13], E. Herrero[1,2], M. Kürster[13], D. Montes[14], E. Nagel[12], V. M. Passegger[12], M. Perger[1,2], A. Rosich[1,2], A. Schweitzer[12], and W. Seifert[6]

[1] Institut de Ciències de l'Espai (ICE, CSIC), Campus UAB, C/ de Can Magrans s/n, 08193 Cerdanyola del Vallès, Spain
e-mail: baroch@ice.cat
[2] Institut d'Estudis Espacials de Catalunya (IEEC), C/ Gran Capità 2-4, 08034 Barcelona, Spain
[3] Institut für Astrophysik, Georg-August-Universität, Friedrich-Hund-Platz 1, 37077 Göttingen, Germany
[4] School of Geosciences, Raymond and Beverly Sackler Faculty of Exact Sciences, Tel Aviv University, 6997801 Tel Aviv, Israel
[5] Departamento de Astrofísica y Ciencias de la Atmósfera, Facultad de Ciencias Físicas, Universidad Complutense de Madrid, 28040 Madrid, Spain
[6] Landessternwarte, Zentrum für Astronomie der Universtät Heidelberg, Königstuhl 12, 69117 Heidelberg, Germany
[7] Centro de Astrobiología (CSIC-INTA), ESAC, Camino Bajo del Castillo s/n, 28692 Villanueva de la Cañada, Madrid, Spain
[8] Instituto de Astrofísica de Canarias, Vía Láctea s/n, 38205 La Laguna, Tenerife, Spain
[9] Departamento de Astrofísica, Universidad de La Laguna, 38026 La Laguna, Tenerife, Spain
[10] Centro Astronómico Hispano Alemán, Observatorio de Calar Alto, Sierra de los Filabres, 04550 Gergal, Spain
[11] Thüringer Landesstenwarte Tautenburg, Sternwarte 5, 07778 Tautenburg, Germany
[12] Hamburger Sternwarte, Gojenbergsweg 112, 21029 Hamburg, Germany
[13] Max-Planck-Institut für Astronomie, Königstuhl 17, 69117 Heidelberg, Germany
[14] Instituto de Astrofísica de Andalucía (IAA-CSIC), Glorieta de la Astronomía s/n, 18008 Granada, Spain

Received 16 May 2018 / Accepted 6 August 2018

ABSTRACT

Context. The CARMENES spectrograph is surveying ~300 M dwarf stars in search for exoplanets. Among the target stars, spectroscopic binary systems have been discovered, which can be used to measure fundamental properties of stars.
Aims. Using spectroscopic observations, we determine the orbital and physical properties of nine new double-line spectroscopic binary systems by analysing their radial velocity curves.
Methods. We use two-dimensional cross-correlation techniques to derive the radial velocities of the targets, which are then employed to determine the orbital properties. Photometric data from the literature are also analysed to search for possible eclipses and to measure stellar variability, which can yield rotation periods.
Results. Out of the 342 stars selected for the CARMENES survey, 9 have been found to be double-line spectroscopic binaries, with periods ranging from 1.13 to ~8000 days and orbits with eccentricities up to 0.54. We provide empirical orbital properties and minimum masses for the sample of spectroscopic binaries. Absolute masses are also estimated from mass-luminosity calibrations, ranging between ~0.1 and ~0.6 $M_{\odot}$.
Conclusions. These new binary systems increase the number of double-line M dwarf binary systems with known orbital parameters by 15%, and they have lower mass ratios on average.

Key words. binaries: spectroscopic – stars: late-type – techniques: radial velocities – techniques: spectroscopic – stars: fundamental parameters – stars: low-mass

1. Introduction

Binary systems are essential for the study of stellar structure and evolution. Depending on their nature, they can yield fundamental properties such as the masses, radii, and luminosities of the components, independently from calibrations and stellar models and with very high precision. This enables critical comparisons with stellar model predictions and the determination of empirical calibrations that can be used for single stars (see Torres et al. 2010, for a review). Due to the increasing interest in the discovery of exoplanets, several instruments were developed to spectroscopically survey a large number of stars. In addition to planetary objects, these projects can also reveal new binary systems that are interesting on their own, because they can be used to constrain the stellar structure and evolution models and to improve the multiplicity statistics of late-type stars (Halbwachs et al. 2003; Mazeh et al. 2003).

This is the case of the CARMENES survey (Quirrenbach et al. 2016). This survey monitors about 300 M dwarf stars to uncover exoplanets in their habitable zones. Targets were selected from available M dwarf catalogues and photometric surveys, and were also carefully studied

to discard unsuitable targets such as visual double systems, known spectroscopic binaries, and very faint stars (see e.g. Alonso-Floriano et al. 2015; Cortés-Contreras et al. 2017; Jeffers et al. 2018, for more details). The CARMENES collaboration has already announced its first planet detections (Reiners et al. 2018a; Sarkis et al. 2018; Trifonov et al. 2018). In addition to the new planets, several spectroscopic binary systems were identified with the first observations of the sample and they were followed-up to characterise them.

The binary systems discovered with CARMENES are especially interesting because the number of known M dwarf binary systems is still scarce (see e.g. the Ninth Catalogue of Spectroscopic Binary Orbits, hereafter SB9[1]; Pourbaix et al. 2004). The distribution of mass ratios and orbital elements may help to understand the formation and evolution of low-mass stars, brown dwarfs, or giant planets in M dwarf stellar systems. Besides, they are also valuable for constraining the properties of M dwarfs, which still show some discrepancies with stellar model predictions (see e.g. Morales et al. 2010; Feiden & Chaboyer 2013, 2014).

In this paper we present nine new double-line spectroscopic binary (SB2) systems discovered in the CARMENES survey. Orbital properties were derived for all of them, yielding their mass ratios and periods for the first time. In Sect. 2 we describe the observations for each system. In Sect. 3.1, the radial velocity analysis of each system is shown. Photometric light curves gathered from the literature and public databases are compiled and discussed in Sect. 3.2. Finally, the results are discussed in Sect. 4 and our conclusions are presented in Sect. 5. Figures of the radial velocity data and the photometric periodogram analysis are compiled in the Appendix.

2. Spectroscopic data

2.1. Spectroscopic observations

High-resolution spectroscopic observations of the targets were taken with the visual (VIS) and near-infrared (NIR) channels of the CARMENES spectrograph from January 2016 to March 2018, covering a wavelength range from 5200 to 9600 Å with a measured resolving power of $R = 94\,600$ in the VIS, and from 9600 to 17100 Å with a measured resolving power of $R = 80\,400$ in the NIR (Quirrenbach et al. 2016). For a few nights when the NIR channel was not available, only VIS spectra are used. From the over 300 studied stars (Reiners et al. 2018b), we have so far identified nine SB2 systems. Between 10 and ~20 observations were taken sampling the orbital phases of short-period systems.

Table 1 lists some basic information for each target. Six publicly available additional HARPS-N (Cosentino et al. 2012) observations were found for one of the systems (Ross 59) and also included in our analysis.

2.2. Radial velocity determination

The candidate spectroscopic binary systems were identified by large variations in their radial velocities, which are routinely calculated by the CARMENES SERVAL pipeline (Caballero et al. 2016b; Zechmeister et al. 2018). This algorithm is based on least-squares fitting of the spectra, providing very accurate radial velocities for single stars (see Anglada-Escudé & Butler 2012). However, it does not yield the velocity of secondary components in binary systems. For that reason, radial velocities of both components were also determined using TODMOR (Zucker 2003), a modern implementation of the two-dimensional (2D) cross-correlation technique TODCOR (Zucker & Mazeh 1994) for multi-order spectra.

To derive the radial velocities of each component of the binary system, we used PHOENIX stellar models (Husser et al. 2013) as templates for the calculation of the cross-correlation functions (CCFs). Using TODMOR, we explored a grid of values for the effective temperatures, flux ratios in the observed wavelength band, and spectral-line broadening to fit all the spectra of each target. Spectral orders with low signal-to-noise ratio (S/N) or telluric contamination were discarded. To obtain the final radial velocity curves of each system in a consistent way, we selected as the template for each system the one that produces the highest CCF peak for spectra with radial velocities obtained close to quadratures. Orbital phases close to conjunction, where the radial velocities of the components cannot be disentangled due to rotational broadening and unfavourable flux ratio, were not considered in this analysis. For this reason, we discarded six spectra for GJ 1029, three for Ross 59, three for GJ 1182 and seven for GJ 810 A in both the VIS and NIR channels. In the case of the VIS spectra, all the parameters could be reliably optimised. However, the effective temperatures resulting from the optimisation process in the NIR spectra always led to unrealistic values at the edge of the grid. Therefore, for the NIR we adopted the values derived from the VIS data and the optimisation was performed on the flux ratio and broadening, which can differ in the NIR channel because of the different wavelength coverage and resolving power.

Only in the case of UU UMi did we use observed spectra as templates with TODMOR, which performed better than synthetic spectra due to the small radial velocity difference between the components and the long period of this system. The co-added spectra of an M2.5 star (Gl 436) and an M5 star (GJ 1253) obtained with CARMENES, were used for the primary and secondary components, respectively. Consequently, the systemic radial velocity derived for UU UMi depends on those of the templates; therefore its uncertainty might be larger. The use of observed spectra does not significantly change the parameters for the other binaries analysed in this work.

Table 2 shows the optimised parameters of the templates for each target, except for UU UMi, for which effective temperatures are obtained from Passegger et al. (2018). These are the parameters used to obtain the radial velocities of the systems with TODMOR, which are provided, together with their uncertainties, in Table A.1.

3. Data analysis

3.1. Radial velocity analysis

The orbital parameters of each target were derived using the SBOP (Etzel 1985) code, which fits the seven parameters of a Keplerian orbit simultaneously to both components: the period ($P_{\rm orb}$), the time of periastron passage (T), the eccentricity (e), and argument of the periastron (ω), the radial velocity semi-amplitudes of each component of the system (K_1 and K_2 for the primary and secondary components, respectively), and the barycentric radial velocity of the system (γ). An initial estimate of the periods was obtained from a Lomb-Scargle periodogram analysis (Scargle 1982) of the radial velocities, and used as input parameter for SBOP.

Although NIR CARMENES measurements have lower precision than those from the VIS channel (Tal-Or et al. 2018), we

[1] http://sb9.astro.ulb.ac.be/

Table 1. Main properties and observing log of the spectroscopic binaries studied in this work.

Name	Karmn	N_{obs}		Δt	Sp.	Ref.[a]	π	G	K_s
		VIS	NIR	(d)	Type		(mas)	(mag)	(mag)
EZ Psc	J00162+198W	10	10	528.6	M4.0V+	AF15	65.72 ± 0.10	10.8968 ± 0.0021	7.083 ± 0.023
GJ 1029	J01056+284	15	15	443.8	M5.0 V+	PMSU	79.84 ± 0.34	12.9701 ± 0.0019	8.550 ± 0.020
Ross 59	J05532+242	22[b]	16	1893.7[b]	M1.5 V+	PMSU	51.5 ± 4.6	9.9176 ± 0.0040	6.633 ± 0.021
NLTT 23956	J10182−204	14	14	359.0	M4.5 V+	Ria06	39.483 ± 0.087	12.3261 ± 0.0025	8.145 ± 0.023
GJ 3612	J10354+694	21	14	686.0	M3.5 V+	PMSU	77.34 ± 0.29	10.7133 ± 0.0019	7.161 ± 0.020
GJ 1182	J14155+046	21	18	428.8	M5.0 V+	PMSU	71.11 ± 0.39	12.6739 ± 0.0020	8.618 ± 0.025
UU UMi	J15412+759	19	18	727.9	M3.0 V+	PMSU	68.3 ± 1.5	11.0493 ± 0.0020	7.442 ± 0.023
LP 395-8	J20198+229	14	12	500.7	M3.0 V+	Lep13	34.081 ± 0.074	10.9990 ± 0.0024	7.283 ± 0.018
GJ 810A	J20556−140N	18	18	556.6	M4.0 V+	PMSU	77.02 ± 0.40	11.0453 ± 0.0024	7.365 ± 0.026

Notes. K_s magnitudes are from the 2MASS survey (Skrutskie et al. 2006). Parallaxes and G magnitudes are from the *Gaia* Data Release 2 (Gaia Collaboration 2016), except for Ross 59, which comes from van Altena et al. (1995). [(a)]AF15: Alonso-Floriano et al. (2015); APASS: Henden et al. (2015); Lep13: Lépine et al. (2013); PMSU: Hawley et al. (1996); Ria06: Riaz et al. (2006); UCAC4: Zacharias et al. (2013). [(b)]Including six additional observations from HARPS-N.

Table 2. Spectral properties of the templates used to derive radial velocities with TODMOR in the VIS and NIR channel spectra.

Name	$T_{eff,1}$ (K)	$T_{eff,2}$ (K)	Spectral-line broadening VIS ($km\,s^{-1}$)	Spectral-line broadening NIR ($km\,s^{-1}$)	L_2/L_1 VIS	L_2/L_1 NIR
EZ Psc	3300 ± 100	2900 ± 100	5.5 ± 0.1	7.1 ± 0.1	0.11 ± 0.01	0.12 ± 0.01
GJ 1029	3100 ± 100	2900 ± 100	4.1 ± 0.1	3.6 ± 0.1	0.24 ± 0.01	0.32 ± 0.01
Ross 59	3900 ± 100	3600 ± 100	1.6 ± 0.1	4.9 ± 0.1	0.10 ± 0.01	0.11 ± 0.01
NLTT 23956	3100 ± 100	3000 ± 100	6.0 ± 0.1	5.9 ± 0.1	0.29 ± 0.01	0.37 ± 0.01
GJ 3612	3600 ± 100	3300 ± 100	2.2 ± 0.1	4.6 ± 0.1	0.21 ± 0.01	0.25 ± 0.01
GJ 1182	3300 ± 100	2900 ± 100	2.4 ± 0.1	4.0 ± 0.1	0.20 ± 0.01	0.29 ± 0.01
UU UMi[a]	3500 ± 51	3300 ± 51	2.6 ± 0.1	6.0 ± 0.1	0.22 ± 0.01	0.27 ± 0.01
LP 395-8	3600 ± 100	3300 ± 100	15.0 ± 0.1	18.1 ± 0.1	0.14 ± 0.01	0.11 ± 0.01
GJ 810A	3400 ± 100	3300 ± 100	4.3 ± 0.1	4.9 ± 0.1	0.61 ± 0.01	0.47 ± 0.01

Notes. Uncertainties indicate the step size used in the grid of models. [(a)]Real templates are used instead of synthetic. Effective temperatures from Passegger et al. (2018).

fitted radial velocities from both channels simultaneously for consistency and considered the respective uncertainties. We also allowed for an adjustable radial velocity jitter ($Jit_{VIS/NIR,1/2}$) in the fit, as defined by Baluev (2009), different for each channel and component. This jitter term represents unaccounted error sources in the estimation of the uncertainties of the measurements. The results show that the jitter parameter of the NIR channel radial velocity of the primary component is always above twice that of the VIS channel, except for LP 395-8. However, in this case, the dispersion of the VIS channel may be affected by the large residual of the observation close to conjunction at orbital phase ~0.8 that does not have a NIR counterpart. Final parameters and uncertainties were computed running the Markov chain Monte Carlo (MCMC) sampler `emcee` (Foreman-Mackey et al. 2013) with a model based on SBOP with additional jitter terms. Parameter uncertainties were derived from the 68.3% credibility interval of the resulting posterior parameter distribution.

The fitted orbital parameters of all targets and their computed physical elements are given in Tables 3 and 4, respectively. Figure B.1 shows the radial velocity fits of all systems. We found three systems in close orbits with periods between 1 and 6 days (EZ Psc, NLTT 23956, and LP 395-8), three systems with intermediate periods between 70 and 160 days (GJ 1029, GJ 3612, and GJ 1182), and three systems with periods longer than about 2 years, for which further measurements are needed to better constrain the parameters (Ross 59, UU UMi, and GJ 810A). All systems show eccentric orbits, with smaller eccentricity in the case of short period binaries, except UU UMi. For this system, due to its long period and the short orbital phase sampled with CARMENES, a circular orbit was assumed in the present work.

3.2. Photometric analysis

To fully characterise our binary systems, we also carried out a bibliographic search for photometric light curves in public archives from surveys such as the Wide Angle Search for Planets (SuperWASP; Pollacco et al. 2006), The MEarth Project (MEarth; Charbonneau et al. 2008; Irwin et al. 2011a; Berta et al. 2012), the All-Sky Automated Survey (ASAS; Pojmański 1997) and the Northern Sky Variability Survey (NSVS; Woźniak et al. 2004). The aim was to search for eclipses in the light curves and the estimation of the rotation period of the systems. Before analysing the photometry we removed outliers as explained in Díez Alonso et al. (1999), iteratively rejecting datapoints deviating more than 2.5σ from the mean of the full photometric dataset for each target. However, outliers were further inspected by eye in order to make sure that possible eclipses were not removed.

Table 3. Radial velocity parameters fitted for each binary system.

Name	P_{orb} (d)	T [JD-2457000]	e	ω (deg)	K_1 (km s^{-1})	K_2 (km s^{-1})	γ (km s^{-1})	σ_1 (km s^{-1})	σ_2 (km s^{-1})	Jit$_{VIS,1}$ (km s^{-1})	Jit$_{NIR,1}$ (km s^{-1})	Jit$_{VIS,2}$ (km s^{-1})	Jit$_{NIR,2}$ (km s^{-1})
EZ Psc	$3.956523^{+0.000071}_{-0.000092}$	$709.24^{+0.25}_{-0.18}$	$0.00220^{+0.00096}_{-0.00090}$	28^{+23}_{-16}	$27.639^{+0.049}_{-0.054}$	$78.56^{+0.23}_{-0.24}$	$-0.501^{+0.031}_{-0.042}$	0.154	0.611	$0.054^{+0.049}_{-0.037}$	$0.43^{+0.22}_{-0.21}$	$0.17^{+0.92}_{-0.80}$	$0.51^{+0.29}_{-0.22}$
GJ 1029	$95.69^{+0.12}_{-0.13}$	$857.31^{+0.45}_{-0.44}$	$0.3859^{+0.0047}_{-0.0048}$	$209.2^{+1.5}_{-1.5}$	$6.799^{+0.041}_{-0.045}$	$9.59^{+0.10}_{-0.10}$	$-11.338^{+0.032}_{-0.032}$	0.485	0.369	$0.033^{+0.037}_{-0.022}$	$0.33^{+0.12}_{-0.10}$	$0.49^{+0.14}_{-0.10}$	$0.23^{+0.14}_{-0.13}$
Ross 59	$721.4^{+2.2}_{-2.0}$	$1006.5^{+1.6}_{-1.5}$	$0.5089^{+0.0089}_{-0.0086}$	$109.2^{+1.7}_{-1.7}$	$2.911^{+0.038}_{-0.039}$	$8.75^{+0.13}_{-0.13}$	$27.496^{+0.021}_{-0.021}$	0.110	0.322	$0.051^{+0.021}_{-0.020}$	$0.200^{+0.086}_{-0.051}$	$0.73^{+0.085}_{-0.050}$	$0.54^{+0.24}_{-0.15}$
NLTT 23956	$5.922845^{+0.000061}_{-0.000059}$	$1007.42^{+0.107}_{-0.094}$	$0.0135^{+0.0012}_{-0.0012}$	$289.1^{+6.4}_{-5.6}$	$32.469^{+0.055}_{-0.056}$	$56.149^{+0.091}_{-0.095}$	$13.688^{+0.033}_{-0.028}$	0.097	0.337	$0.036^{+0.040}_{-0.026}$	$0.14^{+0.108}_{-0.090}$	$0.052^{+0.060}_{-0.037}$	$0.33^{+0.14}_{-0.14}$
GJ 3612	$119.411^{+0.035}_{-0.035}$	$718.42^{+0.57}_{-0.57}$	$0.0655^{+0.0024}_{-0.0024}$	$326.0^{+1.7}_{-1.7}$	$10.638^{+0.028}_{-0.029}$	$20.99^{+0.10}_{-0.10}$	$-62.089^{+0.018}_{-0.018}$	0.147	0.382	$0.025^{+0.026}_{-0.017}$	$0.064^{+0.064}_{-0.050}$	$0.18^{+0.106}_{-0.104}$	$0.451^{+0.121}_{-0.090}$
GJ 1182	$154.24^{+0.12}_{-0.12}$	$867.824^{+0.069}_{-0.070}$	$0.5373^{+0.0016}_{-0.0016}$	$275.76^{+0.28}_{-0.26}$	$11.968^{+0.029}_{-0.028}$	$18.001^{+0.072}_{-0.071}$	$-0.683^{+0.019}_{-0.019}$	0.139	0.370	$0.033^{+0.029}_{-0.023}$	$0.17^{+0.051}_{-0.041}$	$0.064^{+0.066}_{-0.044}$	$0.500^{+0.117}_{-0.088}$
UU UMi	7927^{+847}_{-637}	1118^{+64}_{-44}	0 (fixed)	0 (fixed)	$2.54^{+0.23}_{-0.20}$	$4.46^{+0.22}_{-0.25}$	$-41.17^{+0.20}_{-0.23}$	0.257	0.254	$0.0088^{+0.0089}_{-0.0060}$	$0.421^{+0.090}_{-0.067}$	$0.019^{+0.023}_{-0.014}$	$0.318^{+0.084}_{-0.067}$
LP 395-8	$1.1293392^{+0.0000067}_{-0.0000072}$	$620.075^{+0.038}_{-0.039}$	$0.0071^{+0.0026}_{-0.0022}$	352^{+12}_{-12}	$36.534^{+0.098}_{-0.088}$	$65.29^{+0.19}_{-0.20}$	$-26.616^{+0.056}_{-0.060}$	0.215	0.819	$0.180^{+0.094}_{-0.090}$	$0.095^{+0.135}_{-0.071}$	$0.34^{+0.23}_{-0.21}$	$1.20^{+0.38}_{-0.30}$
GJ 810A	812^{+58}_{-40}	$822.1^{+3.9}_{-3.7}$	$0.402^{+0.059}_{-0.046}$	$238.5^{+1.6}_{-1.7}$	$5.57^{+0.16}_{-0.23}$	$6.74^{+0.19}_{-0.28}$	$-142.098^{+0.021}_{-0.022}$	0.452	0.246	$0.053^{+0.055}_{-0.037}$	$0.63^{+0.18}_{-0.11}$	$0.035^{+0.038}_{-0.024}$	$0.262^{+0.075}_{-0.056}$

Table 4. Physical parameters derived from the radial velocity fits.

Name	$(a_1 + a_2) \sin i$ (au)	$\alpha \sin i$ (mas)	$\mathcal{M}_1 \sin^3 i$ ($M_\odot$)	$\mathcal{M}_2 \sin^3 i$ ($M_\odot$)	$\mathcal{M}_2/\mathcal{M}_1$	$f(\mathcal{M})$ ($10^{-3} M_\odot$)
EZ Psc	$0.038623^{+0.000086}_{-0.000090}$	$2.5393^{+0.0068}_{-0.0070}$	$0.3632^{+0.0027}_{-0.0028}$	$0.12778^{+0.00065}_{-0.00069}$	$0.3518^{+0.0012}_{-0.0013}$	$8.675^{+0.053}_{-0.056}$
GJ 1029	$0.13299^{+0.00091}_{-0.00092}$	$10.618^{+0.085}_{-0.086}$	$0.02005^{+0.00048}_{-0.00049}$	$0.01422^{+0.00025}_{-0.00026}$	$0.7090^{+0.0085}_{-0.0088}$	$2.452^{+0.060}_{-0.064}$
Ross 59	$0.6656^{+0.0085}_{-0.0085}$	$34.3^{+3.1}_{-3.2}$	$0.0567^{+0.0024}_{-0.0024}$	$0.01887^{+0.00066}_{-0.00066}$	$0.3327^{+0.0066}_{-0.0067}$	$1.179^{+0.063}_{-0.063}$
NLTT 23956	$0.048242^{+0.000058}_{-0.000060}$	$1.9048^{+0.0048}_{-0.0048}$	$0.2705^{+0.0010}_{-0.0011}$	$0.15643^{+0.00056}_{-0.00057}$	$0.5783^{+0.0014}_{-0.0014}$	$21.05^{+0.13}_{-0.13}$
GJ 3612	$0.3464^{+0.0011}_{-0.0011}$	$26.79^{+0.13}_{-0.13}$	$0.2581^{+0.0029}_{-0.0029}$	$0.1308^{+0.0010}_{-0.0010}$	$0.5068^{+0.0028}_{-0.0028}$	$14.8^{+1.6}_{-1.6}$
GJ 1182	$0.35835^{+0.00100}_{-0.00099}$	$25.49^{+0.16}_{-0.16}$	$0.1550^{+0.0015}_{-0.0015}$	$0.10305^{+0.00077}_{-0.00077}$	$0.6649^{+0.0031}_{-0.0030}$	$16.47^{+0.16}_{-0.16}$
UU UMi	$5.10^{+0.46}_{-0.38}$	348^{+32}_{-27}	$0.179^{+0.030}_{-0.029}$	$0.102^{+0.020}_{-0.018}$	$0.570^{+0.059}_{-0.055}$	$13.4^{+3.9}_{-3.4}$
LP 395-8	$0.010570^{+0.000022}_{-0.000023}$	$0.3602^{+0.0011}_{-0.0011}$	$0.07920^{+0.00055}_{-0.00057}$	$0.04432^{+0.00026}_{-0.00025}$	$0.5596^{+0.0022}_{-0.0022}$	$5.719^{+0.064}_{-0.056}$
GJ 810A	$0.841^{+0.046}_{-0.038}$	$64.8^{+3.6}_{-3.0}$	$0.0660^{+0.0064}_{-0.0071}$	$0.0545^{+0.0052}_{-0.0056}$	$0.826^{+0.033}_{-0.048}$	$11.2^{+1.3}_{-1.5}$

The rotation period was determined by computing the Lomb-Scargle periodogram (Scargle 1981) of the photometric light curves, and then looking for strong signals between 1 and 200 days (Newton et al. 2016). Uncertainties are estimated as half the full width at half maximum of the periodogram peak, as a conservative approach. To evaluate the significance of the signals, we used the False Alarm Probability (FAP) as described in Scargle (1982), which measures the probability that the signal randomly arises from white noise. Periodic signals with FAP < 0.1% were defined as significant.

We searched for eclipses in the light curves using two different approaches: in the case of binary systems with well determined periods from radial velocities, we folded the light curve of each target in a phase-magnitude diagram using the orbital period found in Sect. 3.1, and checked for a decrease in brightness within a narrow phase region compatible with the radial velocity orbit. We also made use of the Box-fitting Least Squares code (hereafter BLS; Kovács et al. 2002) to identify eclipses with depth similar to the photometric scatter of each curve. BLS was also used in the case of binary systems with poorly constrained periods, although the eclipse probability is very small for long period systems. Both methodologies yielded negative results in all cases and, therefore, we concluded that none of our nine SB2s is an eclipsing binary within the limits of the sampling and measurement accuracy of the photometric data, which are given in Table 5.

Table 5 lists the significant photometric periods found for our targets and the Hα line pseudo-equivalent width resulting from the CARMENES pipeline (Zechmeister et al. 2018) as an indicator of stellar activity (Reid et al. 1995; Hawley et al. 1996). Figure C.1 shows the available photometry, the periodogram, and the light curves phase-folded to the best period found. Significant signals for seven of the systems studied here were found, which we identify as corresponding to the rotation period of the main component (the brightest star) of the systems, assuming that both components may have similar activity levels. Using the same data but with a more conservative approach, Díez Alonso et al. (1999) reported photometric periods for four of our stars (EZ Psc, GJ 3612, UU UMi and LP 395-8). In all cases, the measured P_{rot} are identical within uncertainties.

Interestingly, the three short-period systems (EZ Psc, NLTT 23956, LP 395-8) all have rotation periods below 10 days, and they are active systems showing the Hα line in emission. Furthermore, in these cases the broadening of the spectral lines, which depends on the rotation period of the components and the instrumental resolution, is also larger (see Table 2). However, only in the case of LP 395-8, the binary system with the shortest orbital period, does rotation seem to be pseudo-synchronised with the orbital motion at periastron, although an alias period of ~9 days cannot be excluded with the present data.

The systems EZ Psc and NLTT 23956 seem to be sub-synchronous, with rotation periods larger than their orbital

period. This may indicate that these could be young binary systems still in the process of reaching synchronisation. However, synchronisation timescales are relatively short and even pre-main sequence stars are synchronised for orbital periods below 8–10 days (Mazeh 2008). By statistically analysing the Kepler eclipsing binary candidates, Lurie et al. (2017) suggested that differential rotation could also cause an apparent non-synchronisation of orbital and rotational periods if photospheric active regions are located at higher latitudes, as expected for fast rotation systems (Strassmeier 2002). In their study, they found that 13% of the FGK-type primaries with periods between 2 and 10 days, and with small expected mass ratios, are sub-synchronous, showing a ratio between orbital and rotational period of $P_{\rm orb}/P_{\rm rot} \sim 0.87$. This is not far from the values we would expect for EZ Psc and NLTT 23956 assuming pseudo-synchronisation, $P_{\rm orb}/P_{\rm rot} \sim 0.82$, although smaller.

Although synchronisation is not expected for long-period binary systems, GJ 3612 also shows significant variability with a semi-amplitude of ∼14 mmag and a period of ∼123 days, consistent with the orbital period within uncertainties. However, the rotation period determination may be affected by poor photometric sampling and the narrow time interval covered by the observations and, therefore, interaction between the components cannot be confirmed with the present data.

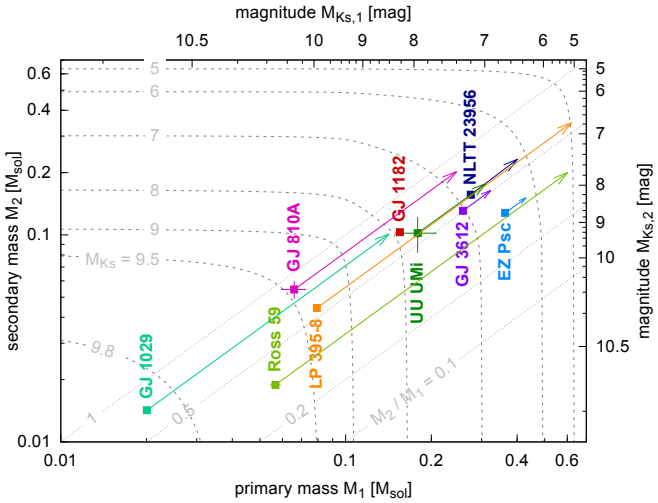

Fig. 1. Minimum masses, $\mathcal{M}\sin^3 i$, for the primary and secondary components of the SB2 binaries (squares). The magnitudes on the top and right axes are computed according to the $\mathcal{M}$–M_{K_s} relation in Benedict et al. (2016). Lines of constant mass ratio values are shown as dotted diagonals. Dashed contours correspond to the same total flux for pairs $M_{K_s,1}$ and $M_{K_s,2}$. The arrows point to the estimated absolute masses and magnitude M_{K_s}. Long arrows are indicative of low orbital inclinations.

4. Results and discussion

4.1. Individual masses and radii

The analysis of the radial velocities of SB2 systems only yields the minimum masses of the components. However, it is possible to estimate absolute values using additional constraints such as mass-luminosity calibrations and mass ratios. We made use of the empirical mass-luminosity relationship ($\mathcal{M}$–M_{K_s}) in Benedict et al. (2016), which is based on mass measurements of astrometric M dwarf binaries. We assumed uncertainties of 0.02 $M_\odot$ according to the scatter of the residuals of this relationship.

To estimate the individual masses, we used the systems' K_s band magnitude of each binary system given in Table 1. From this magnitude and the flux ratio of the system, which we iteratively change between 0 and 1 in steps of 0.01, we computed a set of $K_{s,1}$ and $K_{s,2}$ values corresponding to each component of the system, and converted them to absolute magnitudes $M_{K_{s,1}}$ and $M_{K_{s,2}}$ using the distance of each system. We then determined $\mathcal{M}_1$ and $\mathcal{M}_2$ for each absolute magnitude using the $\mathcal{M}$–M_{K_s} relationship. From the set of possible values, we chose as individual masses those reproducing the mass ratio obtained from the radial velocity analysis, which are listed in Table 4. Alternatively, it is also possible to use the flux ratios derived from the spectral analysis with TODMOR, but in our case, they correspond to the flux ratio at the effective wavelengths of the VIS and NIR CARMENES channels, which have wavelengths shortwards of K_s used for the mass calibration. The second and third columns in Table 6 show the calculated individual masses for each system, with their uncertainties estimated as the standard deviation of 10 000 Monte Carlo realisations of the input parameter distribution.

To check the consistency of individual masses, we compared them with the minimum masses reported in Table 4, finding no discrepant values. Figure 1 shows the minimum masses found for our systems (see Table 4) compared with the $\mathcal{M}$–M_{K_s} calibration from Benedict et al. (2016). The arrows point towards the absolute masses derived from each component (see Table 6). Vertical arrows indicate large inclination angles between the visual and the normal to the orbital plane, while long horizontal arrows indicate systems with low inclination (i.e. small $\sin i$).

Since none of the binary systems presented here are eclipsing, we computed individual radii from individual masses derived in this section and the empirical mass-radius relation in Schweitzer et al. (in prep.), $R = a\mathcal{M} + b$, where $a = 0.934 \pm 0.015$, $b = 0.0286 \pm 0.066$, and R and M are in solar units. This relation is based on masses and radii of eclipsing binaries, and is valid on a mass range from 0.092 $M_\odot$ to 0.73 $M_\odot$. The last two columns in Table 6 provide the individual radii of the components. We have used the radii of the primary components of the binary systems to estimate the inclination of the targets showing rotation periods below 10 days, for which the spectral broadening may be close to the rotation velocity, $v \sin i$. However, only a consistent value of 38 deg was found for LP 395-8, compatible with the lack of eclipses.

4.2. Parameter distribution

We compared our M dwarf SB2 systems with those already reported. We considered the SB9 catalogue of spectroscopic binary orbits (Pourbaix et al. 2004, last update April 2018) which contains the orbital parameters of 3595 spectroscopic binaries, of which 1093 are SB2 systems. Only 18 of these systems correspond to SB2 M dwarf main sequence binary systems. A bibliographic search also results in 40 further known systems with published orbital parameters not included in SB9. Therefore, the nine systems studied in the present work bring the total number of M dwarf SB2 systems to 67, of which 29 are eclipsing, increasing the number of known SB2 systems by 15.5%. Table D.1 compiles the radial velocity parameters for all the 67 spectroscopic binary systems with M dwarf main sequence components we have found in the literature, including the systems analysed in this paper for completeness.

Table 5. Available photometry for the spectroscopic binaries analysed in this work.

Karmn	pEW(Hα) (Å)	Survey	N_{obs} (N_{used}) (#)	Δt (d)	σ (mmag)	P_{rot} (d)	A_λ (mmag)
EZ Psc	-4.16 ± 0.06	MEarth	1660 (1581)	2841	7.5	4.8063 ± 0.0023	3.9
GJ 1029	-0.12 ± 0.02	MEarth	862 (833)	2195	6.1	16.32 ± 0.24	4.3
Ross 59	-0.034 ± 0.001	ASAS	318 (296)	2544	22.4	...	...
NLTT 23956	-7.63 ± 0.09	SuperWASP	14814 (12450)	504	49.9	7.314 ± 0.040	13.3
GJ 3612	0.070 ± 0.008	NSVS	163 (151)	359	19.1	123 ± 15	10.8
GJ 1182	0.10 ± 0.10	MEarth	1203 (1145)	901	4.8	8.92 ± 0.24	1.7
UU UMi	-0.11 ± 0.02	MEarth	1432 (1405)	747	6.6	90 ± 26	2.6
LP 395-8	-3.03 ± 0.16	SuperWASP	986 (880)	67	21.2	1.125 ± 0.011	15.1
GJ 810A	-0.02 ± 0.07	ASAS	417 (394)	3170	65.8	...	...

Notes. Number of observations after 2.5-σ clipping, standard deviation, best period and variability semi-amplitude are listed for each target. Only periods with FAP < 0.1% are given. The pseudo-equivalent width of the Hα line is taken from Jeffers et al. (2018), and is also reported as an activity indicator.

Table 6. Individual masses and absolute magnitudes computed with the mass-luminosity relation in Benedict et al. (2016) and the mass ratio in Table 4, and individual radii computed with the empirical mass-radius relation in Schweitzer et al. (in prep.).

Name	$\mathcal{M}_1$ ($M_\odot$)	$\mathcal{M}_2$ ($M_\odot$)	$\mathcal{R}_1$ ($R_\odot$)	$\mathcal{R}_2$ ($R_\odot$)	$K_{s,1}$ (mag)	$K_{s,2}$ (mag)
EZ Psc	0.430 ± 0.021	0.151 ± 0.020	0.430 ± 0.021	0.170 ± 0.020	6.341 ± 0.023	8.271 ± 0.023
GJ 1029	0.142 ± 0.020	0.101 ± 0.020	0.161 ± 0.020	0.123 ± 0.020	8.407 ± 0.022	9.473 ± 0.038
Ross 59	0.602 ± 0.032	0.200 ± 0.022	0.591 ± 0.032	0.216 ± 0.022	5.31 ± 0.21	7.748 ± 0.084
NLTT 23956	0.401 ± 0.021	0.232 ± 0.020	0.403 ± 0.021	0.245 ± 0.020	6.490 ± 0.025	7.494 ± 0.020
GJ 3612	0.323 ± 0.020	0.164 ± 0.020	0.330 ± 0.021	0.181 ± 0.020	6.914 ± 0.021	8.113 ± 0.023
GJ 1182	0.157 ± 0.020	0.104 ± 0.020	0.175 ± 0.020	0.126 ± 0.020	8.198 ± 0.023	9.359 ± 0.042
UU UMi	0.311 ± 0.024	0.177 ± 0.024	0.319 ± 0.024	0.194 ± 0.024	6.983 ± 0.074	7.98 ± 0.15
LP 395-8	0.621 ± 0.020	0.348 ± 0.020	0.608 ± 0.022	0.353 ± 0.021	5.168 ± 0.021	6.7767 ± 0.0095
GJ 810A	0.245 ± 0.021	0.202 ± 0.021	0.258 ± 0.021	0.217 ± 0.021	7.398 ± 0.036	7.730 ± 0.042

Figure 2 shows the parameter distribution of the SB2 systems in SB9, the M dwarf systems coming from both SB9 and the literature, and our reported new systems (red circles). The SB2s analysed in this work have typically smaller mass ratios than previously published M dwarf binaries. This results from a combination of several factors, including the high S/N and resolution of the CARMENES data, the lower semi-amplitudes induced by less massive components, and our previous literature compilation and preparatory observations, which discarded already-known binary systems from the CARMENES sample of targets (Caballero et al. 2016a; Cortés-Contreras et al. 2017; Jeffers et al. 2018). This initial cleaning also explains the apparently low binary fraction of the sample, with only 9 of the 342 surveyed stars found to be SB2s. In fact, Cortés-Contreras et al. (2017) analysed the CARMENES input catalogue and found a multiplicity fraction of $36.5 \pm 2.6\%$.

Given the orbital periods and separations of the binary systems studied here, it is worth estimating whether or not their orbits could be resolved by *Gaia*, since this would provide precise individual absolute masses independent from calibrations. Using the individual masses in Table 6 and the 1 Gyr stellar models in Baraffe et al. (2015), we estimated individual G-band magnitudes for each component of the systems, which are listed in Table 7. We then computed the semi-major axis of the photocenter motion in the G-band, α_G, shown in the last column in Table 7. We found values ranging from 0.1 to 65 mas; therefore, given the *Gaia* astrometric precision of 50 μas (Lindegren et al. 2018), the astrometric orbits of all systems could be, in principle, resolved. Furthermore, all the binary systems analysed here show an *astrometric excess noise* (Lindegren et al. 2012) parameter above 0.25 mas, always above the median of all the *Gaia* sources (Lindegren et al. 2018). This may indicate that individual astrometric measurements are affected by the orbital motion of the system. Moreover, UU UMi and Ross 59 are flagged as duplicate sources in the second data release, indicating that they may be spatially resolved by *Gaia*.

5. Conclusions

In this work we analysed nine new M dwarf SB2 systems found in the context of the CARMENES survey of exoplanets, increasing the number of known MM spectroscopic binaries by over 15%. Orbital parameters derived from the radial velocities, that is, period, eccentricity, argument of the periastron, radial velocity semi-amplitudes and mass ratios, are provided for these systems for the first time. Among them, three systems have periods shorter than 10 days, three have periods between 70 and 160 days, and three have periods longer than around 2 years for which additional observations may help to better constrain their properties.

Publicly available photometry for these targets was also analysed. Significant periodic signals attributed to the rotation period are found for seven of the systems. Unfortunately, no eclipses are found in any case. However, individual masses and radii were estimated using empirical calibrations for systems with parallactic distances, providing the fundamental properties of the components of the systems.

The comparison of the orbital properties of the systems studied here with those from the literature reveals that our set of low-mass binary systems have smaller mass ratios than more mas-

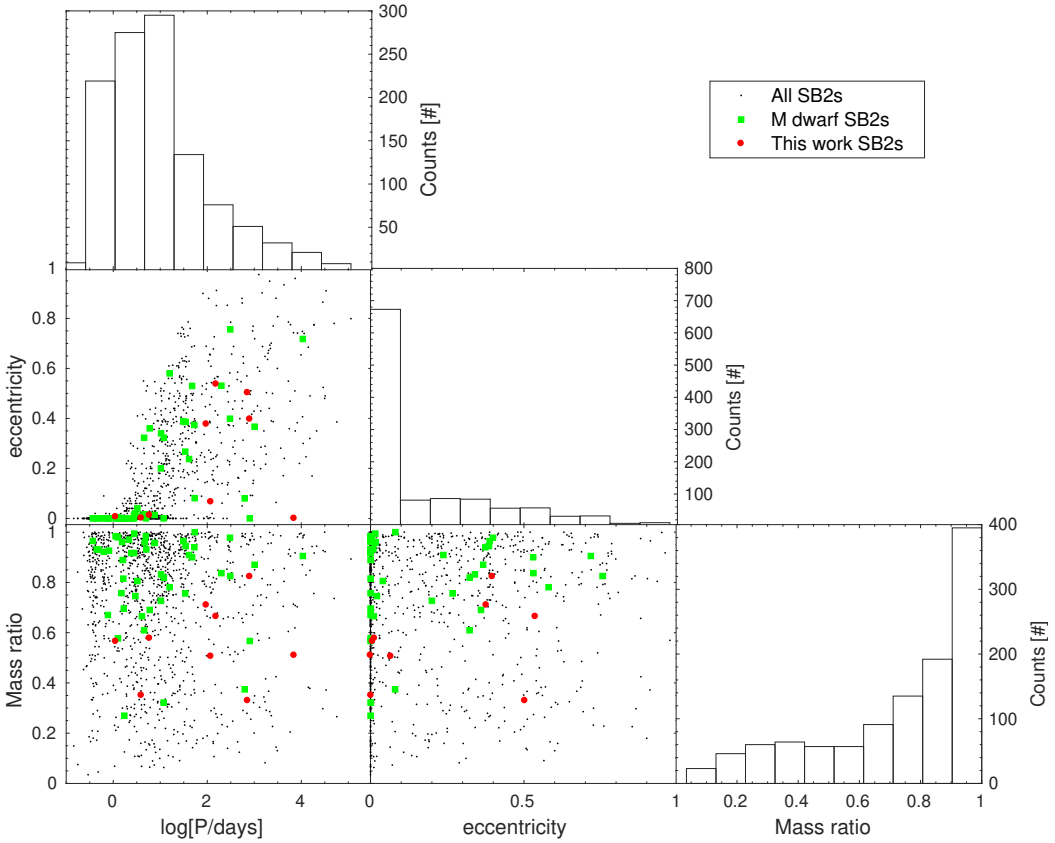

Fig. 2. Parameter distribution of the SB2 spectroscopic binary systems in SB9 (black dots) and in this work (red circles). M dwarf spectroscopic binary systems in SB9 and coming from the literature are also shown as green squares. The *upper panel* of each column displays the one-dimensional distribution of each of parameter.

Table 7. Individual *Gaia G*-band magnitudes estimated using individual masses in Table 6 and the 1 Gyr stellar models in Baraffe et al. (2015), and motion of the semi-major axis of the photocentre in the *G*-band.

Name	G_1 (mag)	G_2 (mag)	α_G (mas)
EZ Psc	11.01	14.28	0.54
GJ 1029	14.60	17.00	3.34
Ross 59	9.24	13.29	7.73
NLTT 23956	11.27	12.92	0.36
GJ 3612	11.94	13.97	5.44
GJ 1182	14.14	16.74	8.05
UU UMi	12.02	13.78	65.2
LP 395-8	8.97	11.70	0.10
GJ 810 A	12.77	13.27	3.97

sive systems and those of known M dwarfs SB2s. This trend may arise from the better sensitivity of the CARMENES spectrograph towards longer wavelengths. This could also suggest that low-mass binary systems may have lower mass ratios, but more statistics are needed to confirm this trend.

Further observations of these systems will help to better constrain the properties of the long-period systems. Precise astrometric measurements from *Gaia* may also be very valuable to put additional constraints and derive absolute masses and inclinations. This will increase the sample of low-mass stars that can be used to refine the mass-luminosity relationship of these systems, independently of stellar models.

Acknowledgements. We are grateful to C. Jordi for useful discussions on *Gaia* data. We also thank the anonymous referee for a thorough and very helpful review of the paper. CARMENES is an instrument for the Centro Astronómico Hispano-Alemán de Calar Alto (CAHA, Almería, Spain). CARMENES is funded by the German Max-Planck-Gesellschaft (MPG), the Spanish Consejo Superior de Investigaciones Científicas (CSIC), the European Union through FEDER/ERF FICTS-2011-02 funds, and the members of the CARMENES Consortium (Max-Planck-Institut für Astronomie, Instituto de Astrofísica de Andalucía, Landessternwarte Königstuhl, Institut de Ciències de l'Espai, Institut für Astrophysik Göttingen, Universidad Complutense de Madrid, Thüringer Landessternwarte Tautenburg, Instituto de Astrofísica de Canarias, Hamburger Sternwarte, Centro de Astrobiología and Centro Astronómico Hispano-Alemán), with additional contributions by the Spanish Ministry of Economy, the German Science Foundation through the Major Research Instrumentation Programme and DFG Research Unit FOR2544 "Blue Planets around Red Stars", the Klaus Tschira Stiftung, the states of Baden-Württemberg and Niedersachsen, and by the Junta de Andalucía. We acknowledge support from the Spanish Ministry of Economy and Competitiveness (MINECO) and the Fondo Europeo de Desarrollo Regional (FEDER) through grants ESP2013-48391-C4-1-R, ESP2014-57495-C2-2-R and AYA2015-69350-C3-2-P, AYA2016-79425–C3–1/2/3–P, ESP2016-80435-C2-1-R, as well as the support of the Generalitat de Catalunya/CERCA programme. We also acknowledge support from the Agència de Gestió d'Ajuts Universitaris i de Recerca of the Generalitat de Catalunya through grant 2018 FI_B_00188. This work makes use of data from the HARPS-N Project, a collaboration between the Astronomical Observatory of the Geneva University (lead), the CfA in Cambridge, the Universities of St. Andrews and Edinburgh, the Queens University of Belfast, and the TNG-INAF Observatory; from the public release of the WASP data as provided by the WASP consortium and services at the NASA Exoplanet Archive, which is operated by the California Institute of Technology, under contract with the National Aeronautics and Space Administration under the Exoplanet Exploration Program; from the MEarth Project, which is a collaboration between Harvard University and the Smithsonian Astrophysical Observatory; and from the Northern Sky Variability Survey created jointly by the Los Alamos National Laboratory and University of Michigan and funded by the Department of Energy, the National Aeronautics and Space Administration, and the National Science Foundation. This work

has made use of data from the European Space Agency (ESA) mission *Gaia* (https://www.cosmos.esa.int/gaia), processed by the *Gaia* Data Processing and Analysis Consortium (DPAC, https://www.cosmos.esa.int/web/gaia/dpac/consortium). Funding for the DPAC has been provided by national institutions, in particular the institutions participating in the *Gaia* Multilateral Agreement.

References

Alonso-Floriano, F. J., Morales, J. C., Caballero, J. A., et al. 2015, A&A, 577, A128
Anglada-Escudé, G., & Butler, R. P. 2012, ApJS, 200, 15
Baluev, R. V. 2009, MNRAS, 393, 969
Baraffe, I., Homeier, D., Allard, F., et al. 2015, A&A, 577, A42
Bayless, A. J., & Orosz, J. A. 2006, ApJ, 651, 1155
Benedict, G. F., Henry, T. J., Franz, O. G., et al. 2016, AJ, 152, 141
Berta, Z. K., Irwin, J., Charbonneau, D., Burke, C. J., & Falco, E. E. 2012, AJ, 144, 145
Birkby, J., Nefs, B., Hodgkin, S., et al. 2012, MNRAS, 426, 1507
Blake, C. H., Torres, G., Bloom, J. S., & Gaudi, B. S. 2008, ApJ, 684, 635
Bopp, B. W., & Fekel, F. C., Jr. 1977, PASP, 89, 65
Caballero, J. A., Cortés-Contreras, M., Alonso-Floriano, F. J., et al. 2016a, in 19th Cambridge Workshop on Cool Stars, Stellar Systems, and the Sun (CS19), 148
Caballero, J. A., Guàrdia, J., López del Fresno, M., et al. 2016b, Proc. SPIE, 9910, 99100E
Charbonneau, D., Irwin, J., & Nutzman, P., & Falco, E. E. 2008, BAAS, 40, 44.02
Cortés-Contreras, M., Béjar, V. J. S., Caballero, J. A., et al. 2017, A&A, 597, A47
Cosentino, R., Lovis, C., Pepe, F., et al. 2012, SPIE Conf. Ser., 8446, 1
Creevey, O. L., Benedict, G. F., Brown, T. M., et al. 2005, ApJ, 625, L127
David, T. J., Hillenbrand, L. A., Cody, A. M., Carpenter, J. M., & Howard, A. W. 2016, ApJ, 816, 21
Delfosse, X., Forveille, T., Beuzit, J.-L., et al. 1999, A&A, 344, 897
Díez Alonso, E., Caballero, J. A., Montes, D., et al. A&A, in press, DOI: 10.1051/0004-6361/201833316
Duquennoy, A., & Mayor, M. 1988, A&A, 200, 135
Etzel, P. B. 1985, SBOP – Spectroscopic Binary Orbit Program (Program's Manual)
Feiden, G., & Chaboyer, B. 2013, ApJ, 779, 183
Feiden, G., & Chaboyer, B. 2014, ApJ, 789, 53
Fekel, F., Jr., Bopp, B. W., & Lacy, C. H. 1978, AJ, 83, 1445
Foreman-Mackey, D., Hogg, D. W., Lang, D., & Goodman, J. 2013, PASP, 125, 306
Forveille, T., Beuzit, J.-L., Delfosse, X., et al. 1999, A&A, 351, 619
Gaia Collaboration (Prusti, T., et al.) 2016, A&A, 595, A1
Gómez Maqueo Chew, Y., Stassun, K. G., Prša, A., et al. 2012, ApJ, 745, 58
Halbwachs, J. L., Mayor, M., Udry, S., & Arenou, F. 2003, A&A, 397, 159
Harlow, J. J. B. 1996, AJ, 112, 2222
Hartman, J. D., Bakos, G. Á., Noyes, R. W., et al. 2011, AJ, 141, 166
Hartman, J. D., Quinn, S. N., Bakos, G. á. et al. 2018, AJ, 155, 114
Hawley, S. L., Gizis, J. E., & Reid, I. N. 1996, AJ, 112, 2799
Hebb, L., Wyse, R. F. G., Gilmore, G., & Holtzman, J. 2006, AJ, 131, 555
Hełminiak, K. G., Konacki, M., Różyczka, M., et al. 2012, MNRAS, 425, 1245
Henden, A. A., Levine, S., Terrell, D., et al. 2015, AAS Meet. Abstracts, 336, 16
Herbig, G. H., & Moorhead, J. M. 1965, ApJ, 141, 649
Husser, T. O., Wende von-Berg, S., Dreizler, S., et al. 2013, A&A, 553, A6
Ireland, M. J., Kraus, A., Martinache, F., Lloyd, J. P., & Tuthill, P. G. 2008, ApJ, 678, 463
Irwin, J., Charbonneau, D., Berta, Z. K., et al. 2009, ApJ, 701, 1436
Irwin, J., Berta, Z. K., Burke, C. J., et al. 2011a, ApJ, 727, 56
Irwin, J. M., Quinn, S. N., Berta, Z. K., et al. 2011b, ApJ, 742, 123
Jeffers, S. V., Schöfer, P., Lamert, A., et al. 2018, A&A, 614, A76
Jeffries, R. D., & Bromage, G. E. 1993, MNRAS, 260, 132
Kovács, G., Zucker, S., & Mazeh, T. 2002, A&A, 391, 369
Kraus, A. L., Tucker, R. A., Thompson, M. I., Craine, E. R., & Hillenbrand, L. A. 2011, ApJ, 728, 48
Kraus, A. L., Douglas, S. T., Mann, A. W., et al. 2017, ApJ, 845, 72
Lépine, S., Hilton, E. J., Mann, A. W., et al. 2013, AJ, 145, 102
Lindegren, L., Lammers, U., Hobbs, D., et al. 2012, A&A, 538, A78
Lindegren, L., Hernandez, J., Bombrun, A., et al. 2018, A&A, 616, A2
López-Morales, M., & Ribas, I. 2005, ApJ, 631, 1120
Lopez-Morales, M., Orosz, J. A., Shaw, J. S., et al. 2006, ApJ, submitted [arXiv:astro-ph/0610225]
Lubin, J. B., Rodriguez, J. E., Zhou, G., et al. 2017, ApJ, 844, 134
Lurie, J. C., Vyhmeister, K., Hawley, S. L., et al. 2017, AJ, 154, 250
Mathieu, R. D., Stassun, K., Basri, G., et al. 1997, AJ, 113, 1841
Mazeh, T. 2008, EAS Pub. Ser., 29, 1
Mazeh, T., Latham, D. W., Goldberg, E., et al. 2001, MNRAS, 325, 343
Mazeh, T., Simon, M., Prato, L., Markus, B., & Zucker, S. 2003, ApJ, 599, 1344
Morales, J. C., Ribas, I., Jordi, C., et al. 2009, ApJ, 691, 1400
Morales, J. C., Gallardo, J., Ribas, I., et al. 2010, ApJ, 718, 502
Nefs, S. V., Birkby, J. L., Snellen, I. A. G., et al. 2013, MNRAS, 431, 3240
Newton, E. R., Irwin, J., Charbonneau, D., et al. 2016, ApJ, 821, 93
Passegger, V. M., Reiners, A., Jeffers, S. V., et al. 2018, A&A, 615, A6
Pojmański, G. 1997, Acta Astron., 47, 467
Pollacco, D. L., Skillen, I., Collier Cameron, A., et al. 2006, PASP, 118, 1407
Pourbaix, D., Tokovinin, A. A., Batten, A. H., et al. 2004, A&A, 424, 727
Quirrenbach, A., Amado, P. J., Caballero, J. A., et al. 2016, Proc. SPIE, 9908, 12
Reid, I. N., Hawley, S. L., & Gizis, J. E. 1995, AJ, 110, 1838
Reiners, A., Ribas, I., Zechmeister, M., et al. 2018a, A&A, 609, L5
Reiners, A., Zechmeister, M., Caballero, J. A., et al. 2018b, A&A, 612, A49
Riaz, B., Gizis, J. E., & Harvin, J. 2006, AJ, 132, 866
Sarkis, P., Henning, T., Kürster, M., et al. 2018, AJ, 155, 257
Scargle, J. D. 1981, ApJS, 45, 1
Scargle, J. D. 1982, ApJ, 263, 835
Skinner, J., Covey, K. R., Bender, C. F., et al. 2018, AJ, 156, 45
Skrutskie, M. F., Cutri, R. M., Stiening, R., et al. 2006, AJ, 131, 1163
Strassmeier, K. G. 2002, Astron. Nachr., 323, 309
Tal-Or, L., Zechmeister, M., Reiners, A., et al. 2018, A&A, 614, A122
Tokovinin, A. A. 1991, A&AS, 91, 497
Tokovinin, A. A. 1994, Astron. Lett., 20, 309
Tokovinin, A. A. 1997, A&AS, 121, 71
Tokovinin, A. A., Balega, Y. Y., Hofmann, K.-H., & Weigelt, G. 2000, Astron. Lett., 26, 668
Tomkin, J., & Pettersen, B. R. 1986, AJ, 92, 1424
Torres, G., & Ribas, I. 2002, ApJ, 567, 1140
Torres, G., Neuhäuser, R., & Guenther, E. W. 2002, AJ, 123, 1701
Torres, G., Andersen, J., & Giménez, A. 2010, A&ARv, 18, 67
Trifonov, T., Kürster, M., Zechmeister, M., et al. 2018, A&A, 609, A117
van Altena, W. F., Lee, J. T., & Hoffleit, E. D. 1995, The general catalogue of trigonometric [stellar] parallaxes (New Haven, CT: Yale University Observatory)
Vogt, S. S., & Fekel, F. J. 1979, ApJ, 234, 958
Woźniak, P. R., Vestrand, W. T., Akerlof, C. W., et al. 2004, ApJ, 127, 2436
Zacharias, N., Finch, C. T., Girard, T. M., et al. 2013, AJ, 145, 44
Zechmeister, M., Reiners, A., Amado, P. J., et al. 2018, A&A, 609, A12
Zhou, G., Bayliss, D., Hartman, J. D., et al. 2015, MNRAS, 451, 2263
Zucker, S. 2003, MNRAS, 342, 1291
Zucker, S., & Mazeh, T. 1994, ApJ, 420, 806

Appendix A: Radial velocity data

Table A.1. Radial velocity measurements.

Name	BJD (2 450 000+)	RV_1 (km s^{-1})	RV_2 (km s^{-1})
Ez Psc	7591.6809	–18.51 ± 0.08	50.71 ± 0.38
(VIS)	7595.6767	–19.85 ± 0.08	54.41 ± 0.38
	7604.6730	–17.19 ± 0.08	47.27 ± 0.35
	7618.5834	14.03 ± 0.09	–41.43 ± 0.37
	7634.5438	8.71 ± 0.09	–26.74 ± 0.40
	7650.6270	–2.40 ± 0.09	6.37 ± 0.34
	7655.5387	–28.11 ± 0.08	78.12 ± 0.34
	7676.4600	6.47 ± 0.08	–20.38 ± 0.37
	7677.5432	25.01 ± 0.09	–73.18 ± 0.39
	8120.2882	26.57 ± 0.08	–77.31 ± 0.37
Ez Psc	7591.6810	–18.57 ± 0.14	51.51 ± 0.46
(NIR)	7595.6779	–20.17 ± 0.16	54.12 ± 0.41
	7604.6730	–17.38 ± 0.15	47.52 ± 0.38
	7618.5845	13.84 ± 0.15	–42.25 ± 0.43
	7634.5464	8.50 ± 0.17	–26.00 ± 0.61
	7650.6280	–2.61 ± 0.15	5.69 ± 0.31
	7655.5384	–28.40 ± 0.16	76.52 ± 0.63
	7676.4601	6.33 ± 0.18	–20.77 ± 0.56
	7677.5434	24.87 ± 0.14	–72.71 ± 0.57
	8120.2883	26.14 ± 0.16	–76.99 ± 0.59
GJ 1029	7611.6660	–7.11 ± 0.09	–17.00 ± 0.24
(VIS)	7619.6197	–7.81 ± 0.10	–16.46 ± 0.22
	7620.6000	–7.95 ± 0.10	–16.40 ± 0.22
	7625.5827	–8.69 ± 0.10	–16.15 ± 0.23
	7786.3730	–7.13 ± 0.12	–16.86 ± 0.30
	7936.6348	–15.13 ± 0.09	–5.92 ± 0.23
	7951.6386	–20.17 ± 0.10	0.88 ± 0.29
	7981.6498	–6.86 ± 0.09	–17.15 ± 0.25
	7999.6108	–7.59 ± 0.09	–16.62 ± 0.22
	8031.5371	–14.89 ± 0.09	–6.34 ± 0.22
	8033.5194	–15.66 ± 0.10	–5.34 ± 0.26
	8040.4951	–19.03 ± 0.10	–0.66 ± 0.27
	8047.4815	–20.11 ± 0.09	0.87 ± 0.27
	8051.4670	–17.52 ± 0.09	–2.52 ± 0.25
	8055.4708	–14.22 ± 0.10	–6.74 ± 0.26
GJ 1029	7611.6661	–7.42 ± 0.16	–17.18 ± 0.34
(NIR)	7619.6204	–8.41 ± 0.22	–15.70 ± 0.44
	7620.6000	–8.51 ± 0.19	–15.36 ± 0.34
	7625.5824	–9.18 ± 0.16	–14.90 ± 0.28
	7786.3723	–7.58 ± 0.22	–17.18 ± 0.43
	7936.6348	–14.16 ± 0.14	–5.81 ± 0.27
	7951.6386	–19.49 ± 0.13	1.81 ± 0.28
	7981.6496	–7.11 ± 0.15	–17.40 ± 0.31
	7999.6106	–8.19 ± 0.16	–16.49 ± 0.34
	8031.5359	–14.23 ± 0.14	–6.94 ± 0.30
	8033.5196	–15.33 ± 0.17	–5.38 ± 0.35
	8040.4955	–19.04 ± 0.14	–0.40 ± 0.30
	8047.4813	–20.13 ± 0.13	1.12 ± 0.29
	8051.4666	–17.38 ± 0.14	–2.42 ± 0.30
	8055.4693	–13.64 ± 0.16	–7.96 ± 0.31
Ross 59	6255.6871	28.32 ± 0.07	23.97 ± 0.62
(HARPS-N)	6255.7830	28.33 ± 0.08	24.12 ± 0.65
	6604.6893	24.04 ± 0.07	37.34 ± 1.09
	6605.6889	24.04 ± 0.07	37.50 ± 0.82
	6606.6984	24.04 ± 0.07	37.08 ± 0.95
	6607.6778	24.04 ± 0.07	37.33 ± 0.98
Ross 59	7652.6555	28.07 ± 0.03	25.59 ± 0.24
(VIS)	7656.6492	28.08 ± 0.03	25.52 ± 0.24
	7676.6923	28.23 ± 0.03	25.03 ± 0.20
	7689.6558	28.35 ± 0.04	24.63 ± 0.31
	7691.6467	28.36 ± 0.03	24.65 ± 0.18
	7692.6448	28.34 ± 0.03	24.48 ± 0.19
	7693.6418	28.35 ± 0.03	24.49 ± 0.22
	7701.6213	28.46 ± 0.04	24.49 ± 0.26
	7766.5483	29.01 ± 0.03	23.04 ± 0.19
	7815.3666	29.46 ± 0.02	21.91 ± 0.16
	7830.4308	29.58 ± 0.03	21.50 ± 0.18
	7851.3390	29.80 ± 0.03	21.03 ± 0.21
	8017.6101	25.18 ± 0.03	34.67 ± 0.20
	8088.6191	24.54 ± 0.03	36.61 ± 0.20
	8118.4902	24.98 ± 0.03	35.07 ± 0.16
	8149.4038	25.51 ± 0.03	33.71 ± 0.18
Ross 59	7766.5484	28.84 ± 0.06	22.14 ± 0.17
(NIR)	7815.3670	29.33 ± 0.05	21.84 ± 0.17
	7830.4318	29.44 ± 0.06	21.73 ± 0.19
	7851.3392	29.71 ± 0.07	21.29 ± 0.33
	8017.6116	25.59 ± 0.05	34.40 ± 0.28
	8088.6191	24.51 ± 0.10	36.47 ± 0.41
	8118.4902	25.06 ± 0.07	34.13 ± 0.33
	8149.4025	25.57 ± 0.07	32.92 ± 0.19
NLTT 23956	7735.7087	43.19 ± 0.13	–37.45 ± 0.19
(VIS)	7799.5416	4.10 ± 0.13	30.29 ± 0.21
	7814.4799	18.19 ± 0.13	6.49 ± 0.21
	7821.4617	–12.76 ± 0.13	59.86 ± 0.19
	7830.4822	43.27 ± 0.14	–37.63 ± 0.20
	7832.4844	10.38 ± 0.13	19.63 ± 0.19
	7848.4245	45.39 ± 0.13	–40.90 ± 0.21
	7850.3877	5.73 ± 0.14	27.13 ± 0.21
	7856.3647	4.15 ± 0.14	30.29 ± 0.22
	7861.3722	33.45 ± 0.14	–20.22 ± 0.20
	7866.3890	46.20 ± 0.14	–42.50 ± 0.21
	8080.7339	26.90 ± 0.14	–9.02 ± 0.20
	8092.7091	22.71 ± 0.13	–2.18 ± 0.19
	8094.7477	–17.47 ± 0.13	67.61 ± 0.18
NLTT 23956	7735.7080	43.30 ± 0.19	–37.46 ± 0.30
(NIR)	7799.5416	4.07 ± 0.20	30.74 ± 0.30
	7814.4798	18.15 ± 0.20	6.67 ± 0.31
	7821.4619	–12.90 ± 0.18	59.38 ± 0.29
	7830.4824	43.35 ± 0.21	–37.85 ± 0.33
	7832.4845	10.44 ± 0.22	18.57 ± 0.30
	7848.4241	45.42 ± 0.20	–41.07 ± 0.30
	7850.3878	5.64 ± 0.31	26.98 ± 0.45
	7856.3646	3.94 ± 0.24	30.00 ± 0.35
	7861.3722	33.36 ± 0.22	–20.42 ± 0.34
	7866.3885	46.05 ± 0.28	–42.43 ± 0.46
	8080.7338	27.00 ± 0.33	–9.47 ± 0.50
	8092.7084	22.77 ± 0.21	–2.13 ± 0.32
	8094.7472	–17.60 ± 0.24	67.59 ± 0.31
GJ 3612	7419.6610	–70.23 ± 0.07	–46.10 ± 0.25
(VIS)	7474.4705	–54.91 ± 0.07	–76.35 ± 0.26
	7494.4779	–51.12 ± 0.07	–83.26 ± 0.27

Table A.1. continued.

Name	BJD (2 450 000+)	RV_1 (km s^{-1})	RV_2 (km s^{-1})
	7672.7357	–72.14 ± 0.08	–42.13 ± 0.27
	7690.6364	–67.61 ± 0.07	–51.27 ± 0.23
	7709.5717	–56.88 ± 0.07	–72.03 ± 0.25
	7759.5694	–62.78 ± 0.10	–60.47 ± 0.33
	7761.6902	–63.70 ± 0.08	–58.34 ± 0.30
	7762.5343	–64.08 ± 0.07	–57.64 ± 0.25
	7763.6222	–64.59 ± 0.07	–56.92 ± 0.23
	7766.5875	–65.93 ± 0.07	–54.60 ± 0.26
	7787.5680	–72.05 ± 0.07	–42.33 ± 0.25
	7802.7532	–70.42 ± 0.07	–45.70 ± 0.25
	7815.7454	–64.75 ± 0.08	–56.77 ± 0.25
	7819.7395	–62.71 ± 0.11	–60.59 ± 0.36
	7823.4053	–60.12 ± 0.08	–66.54 ± 0.26
	7830.6792	–55.93 ± 0.07	–73.98 ± 0.27
	7833.3296	–54.62 ± 0.07	–76.98 ± 0.26
	7850.5303	–51.01 ± 0.07	–84.04 ± 0.26
	8088.7086	–50.96 ± 0.08	–84.04 ± 0.29
	8105.7093	–56.30 ± 0.07	–73.22 ± 0.27
GJ 3612 (NIR)	7474.4704	–55.37 ± 0.07	–76.48 ± 0.18
	7672.7355	–72.35 ± 0.07	–42.68 ± 0.17
	7690.6361	–67.82 ± 0.09	–51.42 ± 0.26
	7709.5699	–56.95 ± 0.08	–72.16 ± 0.22
	7763.6248	–64.56 ± 0.08	–57.30 ± 0.17
	7766.5882	–66.06 ± 0.07	–54.88 ± 0.18
	7787.5640	–72.21 ± 0.08	–42.67 ± 0.22
	7802.7533	–70.49 ± 0.07	–45.81 ± 0.19
	7815.7448	–64.65 ± 0.11	–57.03 ± 0.22
	7823.4070	–60.66 ± 0.07	–67.05 ± 0.14
	7830.6779	–56.01 ± 0.08	–74.42 ± 0.22
	7833.3285	–55.00 ± 0.07	–76.86 ± 0.17
	8088.7084	–51.06 ± 0.14	–84.19 ± 0.36
	8105.7097	–56.46 ± 0.10	–73.54 ± 0.23
GJ 1182 (VIS)	7488.5925	–2.53 ± 0.08	2.18 ± 0.23
	7494.5471	–3.28 ± 0.08	3.34 ± 0.19
	7505.5087	–5.12 ± 0.08	6.02 ± 0.22
	7802.6332	–3.34 ± 0.07	3.30 ± 0.18
	7822.6421	–6.80 ± 0.07	8.54 ± 0.19
	7833.6210	–9.04 ± 0.07	11.87 ± 0.20
	7848.5930	–11.69 ± 0.07	15.97 ± 0.21
	7850.5784	–11.86 ± 0.07	16.31 ± 0.20
	7854.6329	–11.88 ± 0.07	16.31 ± 0.20
	7858.5516	–10.87 ± 0.08	14.52 ± 0.21
	7860.5355	–9.69 ± 0.08	12.68 ± 0.21
	7862.5431	–7.58 ± 0.08	9.57 ± 0.21
	7864.5170	–4.87 ± 0.09	5.52 ± 0.25
	7875.5984	11.00 ± 0.08	–18.30 ± 0.20
	7888.5064	10.53 ± 0.07	–17.71 ± 0.20
	7889.5389	10.28 ± 0.08	–17.34 ± 0.22
	7894.4574	9.11 ± 0.07	–15.34 ± 0.20
	7901.4802	7.34 ± 0.08	–13.06 ± 0.22
	7907.4334	5.91 ± 0.07	–10.27 ± 0.22
	7912.4396	4.86 ± 0.08	–8.71 ± 0.21
	7917.4318	3.85 ± 0.08	–7.08 ± 0.23

Table A.1. continued.

Name	BJD (2 450 000+)	RV_1 (km s^{-1})	RV_2 (km s^{-1})
GJ 1182 (NIR)	7488.6016	–2.23 ± 0.08	3.59 ± 0.17
	7802.6334	–2.95 ± 0.12	3.87 ± 0.18
	7822.6418	–7.00 ± 0.09	8.43 ± 0.18
	7833.6206	–9.18 ± 0.09	11.59 ± 0.17
	7848.5927	–11.81 ± 0.11	15.89 ± 0.22
	7852.5741	–12.19 ± 0.08	16.13 ± 0.17
	7854.6322	–12.07 ± 0.13	15.97 ± 0.24
	7858.5532	–11.04 ± 0.09	14.38 ± 0.17
	7860.5360	–9.85 ± 0.11	12.57 ± 0.21
	7862.5435	–7.89 ± 0.08	9.67 ± 0.18
	7875.5984	10.82 ± 0.11	–18.71 ± 0.22
	7888.5058	10.57 ± 0.10	–17.53 ± 0.20
	7889.5374	10.31 ± 0.12	–17.14 ± 0.23
	7894.4546	9.22 ± 0.10	–15.19 ± 0.19
	7901.4794	6.93 ± 0.13	–13.19 ± 0.25
	7907.4328	5.82 ± 0.12	–10.84 ± 0.24
	7912.4389	4.75 ± 0.09	–8.97 ± 0.19
	7917.4175	3.63 ± 0.11	–7.63 ± 0.21
UU UMi (VIS)	7472.6413	–38.92 ± 0.02	–44.98 ± 0.09
	7504.5670	–38.94 ± 0.03	–45.06 ± 0.09
	7529.4912	–38.90 ± 0.03	–45.12 ± 0.10
	7556.4629	–38.87 ± 0.03	–45.15 ± 0.11
	7559.5434	–38.91 ± 0.03	–45.18 ± 0.11
	7763.6439	–38.75 ± 0.03	–45.46 ± 0.10
	7800.7530	–38.71 ± 0.02	–45.52 ± 0.09
	7815.5392	–38.68 ± 0.03	–45.51 ± 0.09
	7832.5606	–38.67 ± 0.03	–45.50 ± 0.10
	7848.6126	–38.71 ± 0.03	–45.53 ± 0.09
	7867.5390	–38.65 ± 0.03	–45.53 ± 0.11
	7897.4662	–38.67 ± 0.03	–45.52 ± 0.11
	7931.5387	–38.64 ± 0.03	–45.57 ± 0.13
	7961.3985	–38.62 ± 0.03	–45.61 ± 0.12
	7993.3479	–38.61 ± 0.03	–45.64 ± 0.15
	8054.3032	–38.65 ± 0.03	–45.65 ± 0.10
	8117.7403	–38.67 ± 0.03	–45.66 ± 0.09
	8161.7033	–38.65 ± 0.03	–45.64 ± 0.10
	8200.5577	–38.60 ± 0.03	–45.60 ± 0.11
UU UMi (NIR)	7472.6401	–39.33 ± 0.06	–45.45 ± 0.12
	7504.5679	–39.19 ± 0.07	–45.33 ± 0.12
	7529.4903	–39.29 ± 0.06	–45.42 ± 0.10
	7556.4628	–39.70 ± 0.08	–45.90 ± 0.14
	7559.5432	–38.92 ± 0.07	–45.12 ± 0.11
	7763.6438	–39.06 ± 0.08	–45.60 ± 0.16
	7800.7531	–39.11 ± 0.06	–45.70 ± 0.13
	7815.5387	–39.02 ± 0.06	–45.65 ± 0.13
	7832.5591	–39.07 ± 0.06	–45.65 ± 0.13
	7848.6135	–39.03 ± 0.08	–45.61 ± 0.16
	7867.5386	–38.97 ± 0.06	–45.60 ± 0.14
	7897.4628	–38.67 ± 0.07	–45.29 ± 0.14
	7931.5379	–38.73 ± 0.06	–45.36 ± 0.16
	7961.3982	–38.03 ± 0.09	–44.70 ± 0.20
	7993.3477	–38.56 ± 0.11	–45.08 ± 0.24
	8054.3030	–39.33 ± 0.09	–45.97 ± 0.25
	8117.7404	–39.05 ± 0.09	–45.66 ± 0.17
	8200.5573	–39.06 ± 0.13	–45.34 ± 0.24

Table A.1. continued.

Name	BJD (2 450 000+)	RV_1 (km s^{-1})	RV_2 (km s^{-1})
LP 395-8 (VIS)	7545.6530	5.91 ± 0.16	–84.53 ± 0.31
	7566.6209	–49.26 ± 0.18	12.96 ± 0.36
	7573.5523	–20.07 ± 0.20	–39.89 ± 0.41
	7593.4966	–60.67 ± 0.18	34.48 ± 0.32
	7633.4363	–14.10 ± 0.25	–49.58 ± 0.58
	7643.4056	–50.69 ± 0.17	16.70 ± 0.31
	7652.3889	–57.38 ± 0.22	28.04 ± 0.43
	7652.4062	–55.33 ± 0.25	25.16 ± 0.47
	7652.4215	–53.40 ± 0.18	21.52 ± 0.49
	7652.4367	–51.37 ± 0.17	17.13 ± 0.31
	7654.3796	–48.09 ± 0.20	13.25 ± 0.35
	8089.2778	–60.97 ± 0.28	34.54 ± 0.87
	8093.2694	10.16 ± 0.13	–91.82 ± 0.26
	8102.2775	8.98 ± 0.17	–90.36 ± 0.32
LP 395-8 (NIR)	7545.6508	5.83 ± 0.19	–84.06 ± 0.35
	7593.4976	–60.46 ± 0.26	33.66 ± 0.59
	7633.4363	–14.19 ± 0.40	–46.36 ± 0.55
	7643.4069	–50.66 ± 0.24	15.68 ± 0.45
	7652.3889	–57.74 ± 0.50	27.92 ± 0.98
	7652.4063	–55.93 ± 0.49	25.07 ± 1.36
	7652.4216	–53.72 ± 0.29	22.93 ± 0.50
	7652.4353	–51.50 ± 0.24	18.49 ± 0.42
	7654.3791	–48.37 ± 0.27	12.20 ± 0.49
	8089.2780	–60.99 ± 0.76	33.26 ± 1.32
	8093.2686	9.75 ± 0.24	–90.38 ± 0.65
	8102.2776	9.08 ± 0.44	–89.16 ± 1.46

Table A.1. continued.

Name	BJD (2 450 000+)	RV_1 (km s^{-1})	RV_2 (km s^{-1})
GJ 810A (VIS)	7626.5156	–144.98 ± 0.12	–138.40 ± 0.14
	7630.4562	–145.09 ± 0.12	–138.25 ± 0.14
	7642.4209	–145.54 ± 0.10	–137.85 ± 0.12
	7652.3733	–146.00 ± 0.13	–137.62 ± 0.15
	7655.4534	–145.94 ± 0.11	–137.40 ± 0.12
	7673.3313	–146.57 ± 0.11	–136.80 ± 0.12
	7677.3211	–146.70 ± 0.11	–136.59 ± 0.13
	7704.2706	–147.54 ± 0.10	–135.56 ± 0.12
	7911.6195	–138.92 ± 0.12	–146.13 ± 0.12
	7928.5978	–138.42 ± 0.11	–146.59 ± 0.12
	7943.5924	–138.08 ± 0.12	–146.90 ± 0.13
	7958.5804	–137.85 ± 0.10	–147.18 ± 0.12
	7975.5164	–137.60 ± 0.11	–147.31 ± 0.12
	7990.4604	–137.54 ± 0.11	–147.36 ± 0.13
	8020.3798	–137.62 ± 0.11	–147.36 ± 0.12
	8048.3226	–137.83 ± 0.11	–147.13 ± 0.12
	8089.2567	–138.58 ± 0.12	–146.74 ± 0.13
	8093.2450	–138.62 ± 0.11	–146.66 ± 0.12
GJ 810A (NIR)	7626.5157	–143.92 ± 0.14	–138.14 ± 0.16
	7630.4562	–144.10 ± 0.15	–138.16 ± 0.15
	7652.3734	–145.31 ± 0.32	–137.77 ± 0.33
	7655.4529	–145.62 ± 0.15	–137.95 ± 0.14
	7673.3310	–146.40 ± 0.13	–136.75 ± 0.14
	7677.3211	–146.72 ± 0.17	–136.72 ± 0.20
	7704.2692	–147.59 ± 0.16	–135.49 ± 0.17
	7928.5971	–139.18 ± 0.13	–146.65 ± 0.13
	7943.5931	–138.37 ± 0.18	–146.70 ± 0.17
	7958.5790	–137.46 ± 0.14	–146.58 ± 0.15
	7975.5159	–137.72 ± 0.15	–147.29 ± 0.16
	7990.4607	–137.68 ± 0.15	–147.29 ± 0.15
	8020.3803	–137.54 ± 0.14	–147.12 ± 0.14
	8048.3221	–138.46 ± 0.14	–147.44 ± 0.15
	7911.6058	–139.92 ± 0.12	–146.24 ± 0.12
	8074.2568	–139.03 ± 0.16	–147.09 ± 0.17
	8089.2560	–139.25 ± 0.45	–147.44 ± 0.50
	8093.2439	–139.10 ± 0.15	–146.51 ± 0.16

Appendix B: Radial velocity data fits

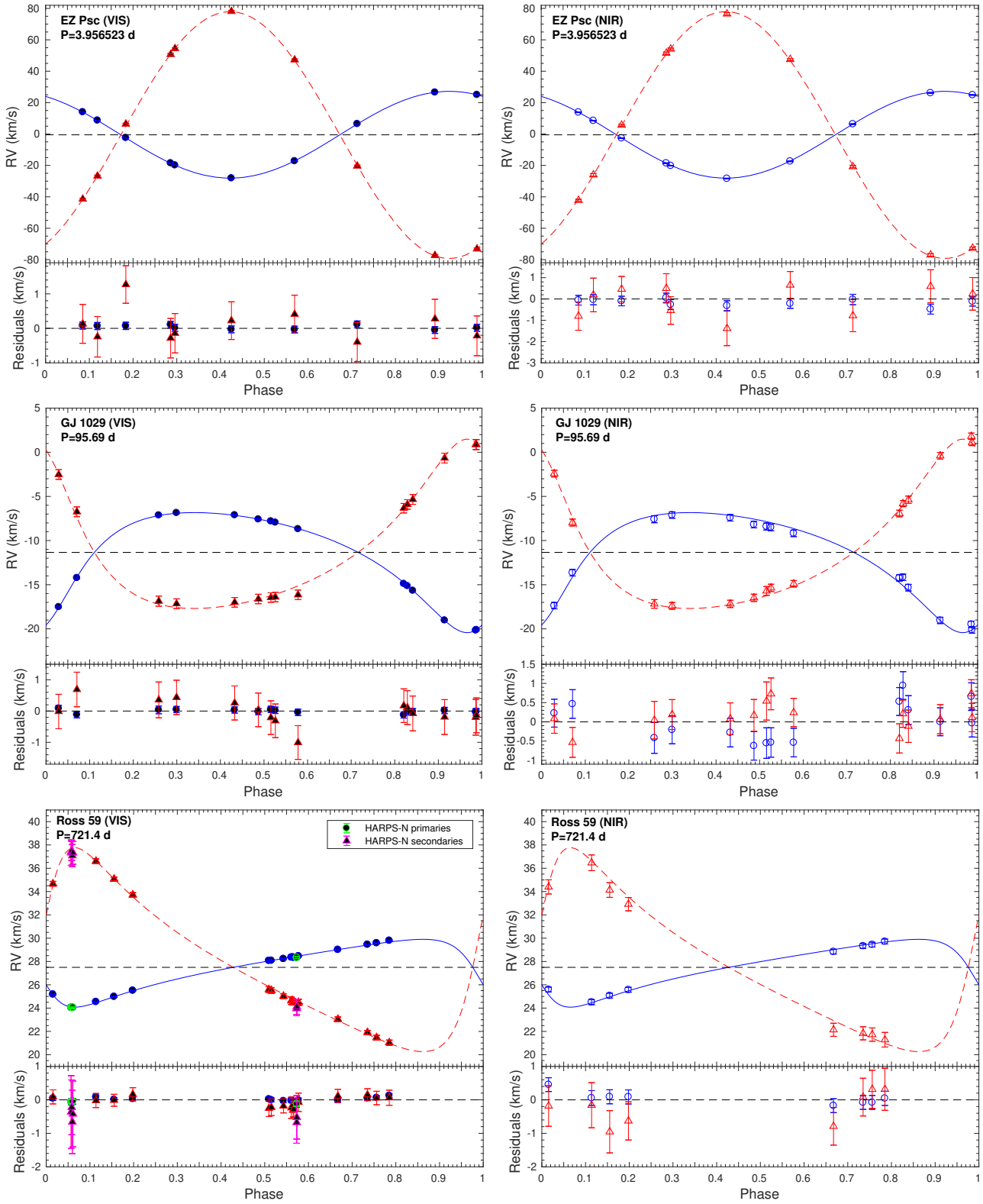

Fig. B.1. Radial velocity curves of our targets as a function of the orbital phase. VIS and NIR CARMENES data are shown in the *left* and *right panels*, respectively, for each target as labelled. The top plot in each panel displays the radial velocity data of the primary (blue circle) and secondary (red triangle) components, along with their best-fitting models (blue solid and red dashed lines, respectively). The bottom plot on each panel shows the residuals of the best fit. For Ross 59, HARPS data for the primary (green circles) and secondary (violet triangles) are also shown.

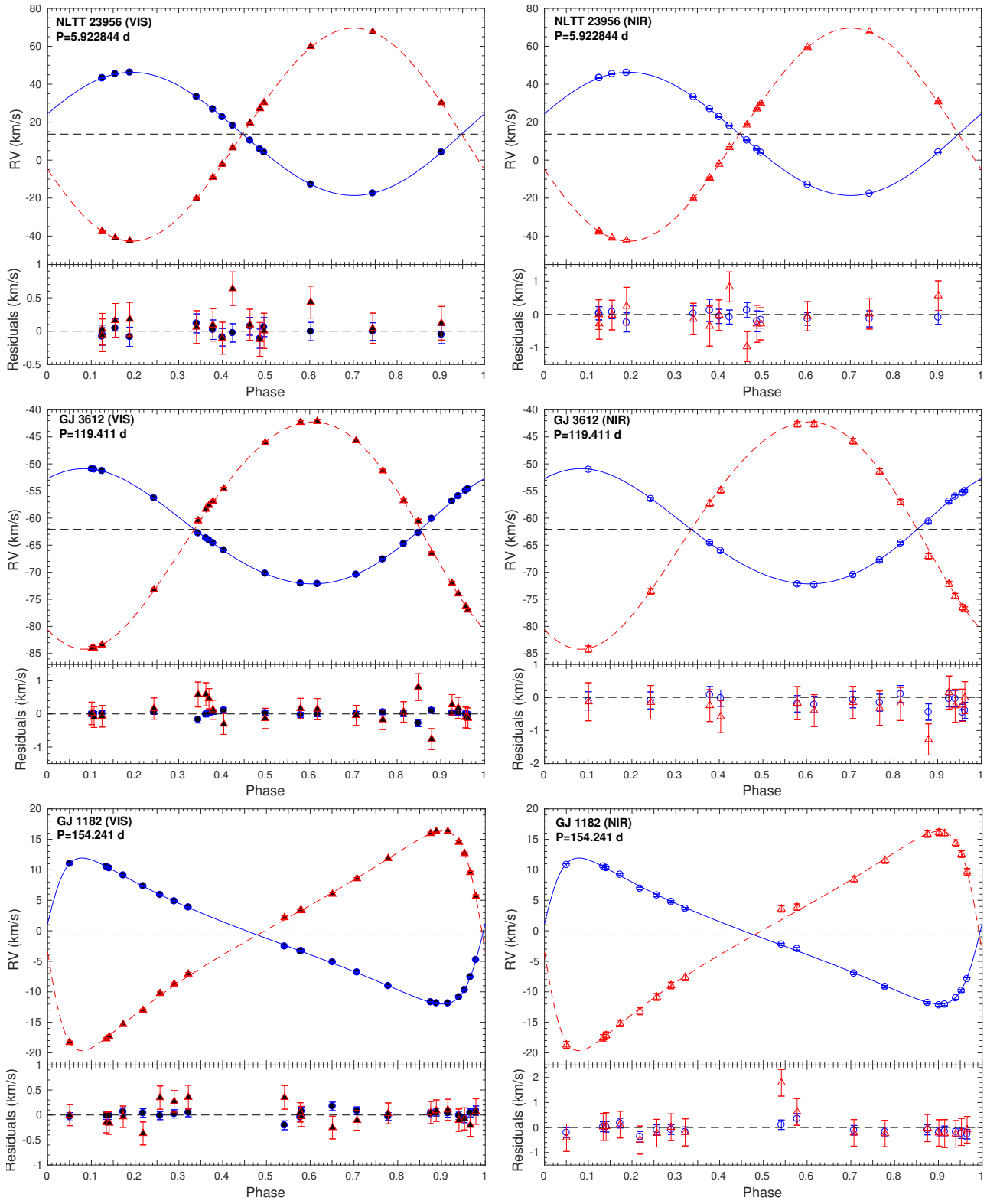

Fig. B.1. continued.

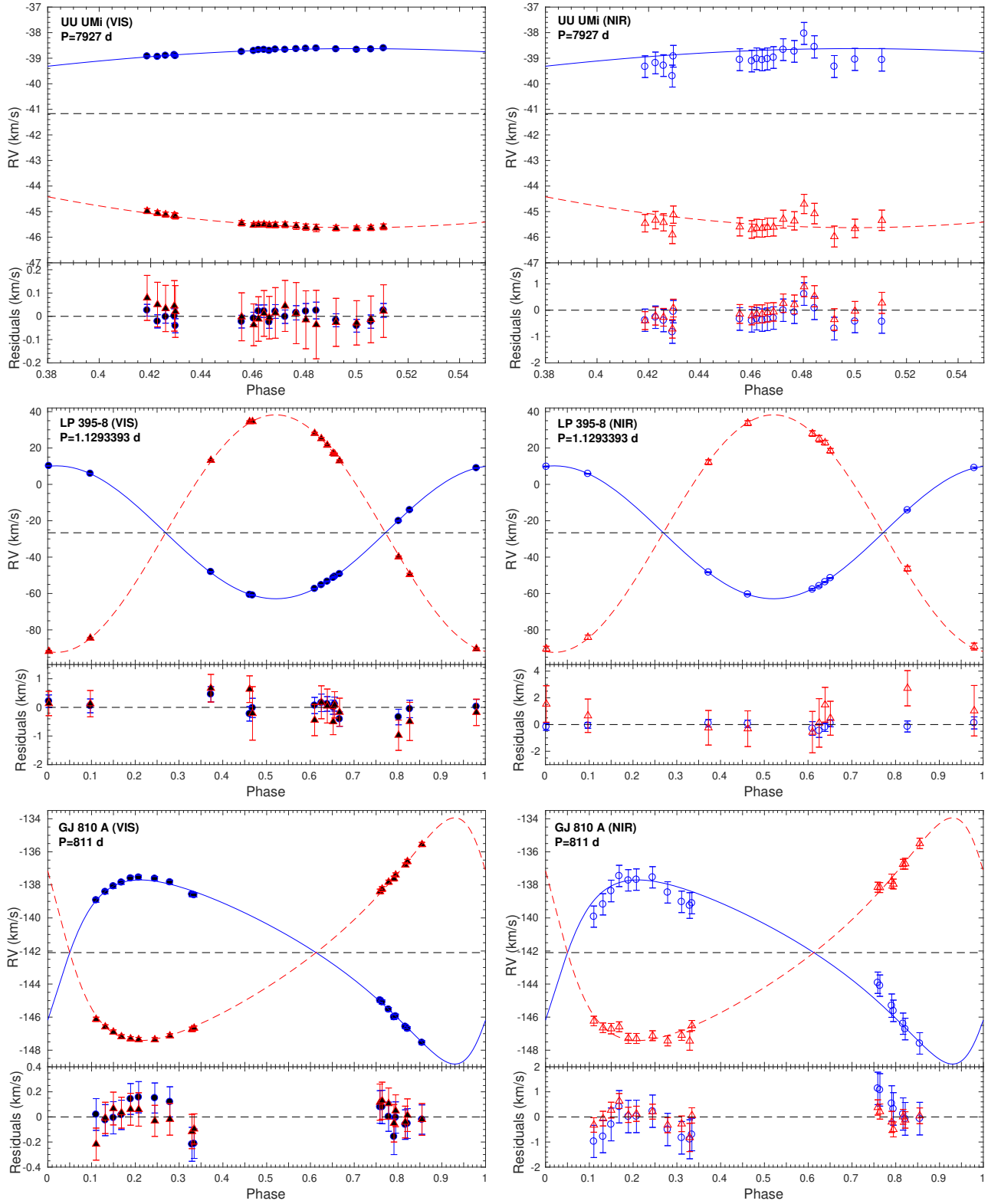

Fig. B.1. continued.

Appendix C: Photometric data and periodogram analysis

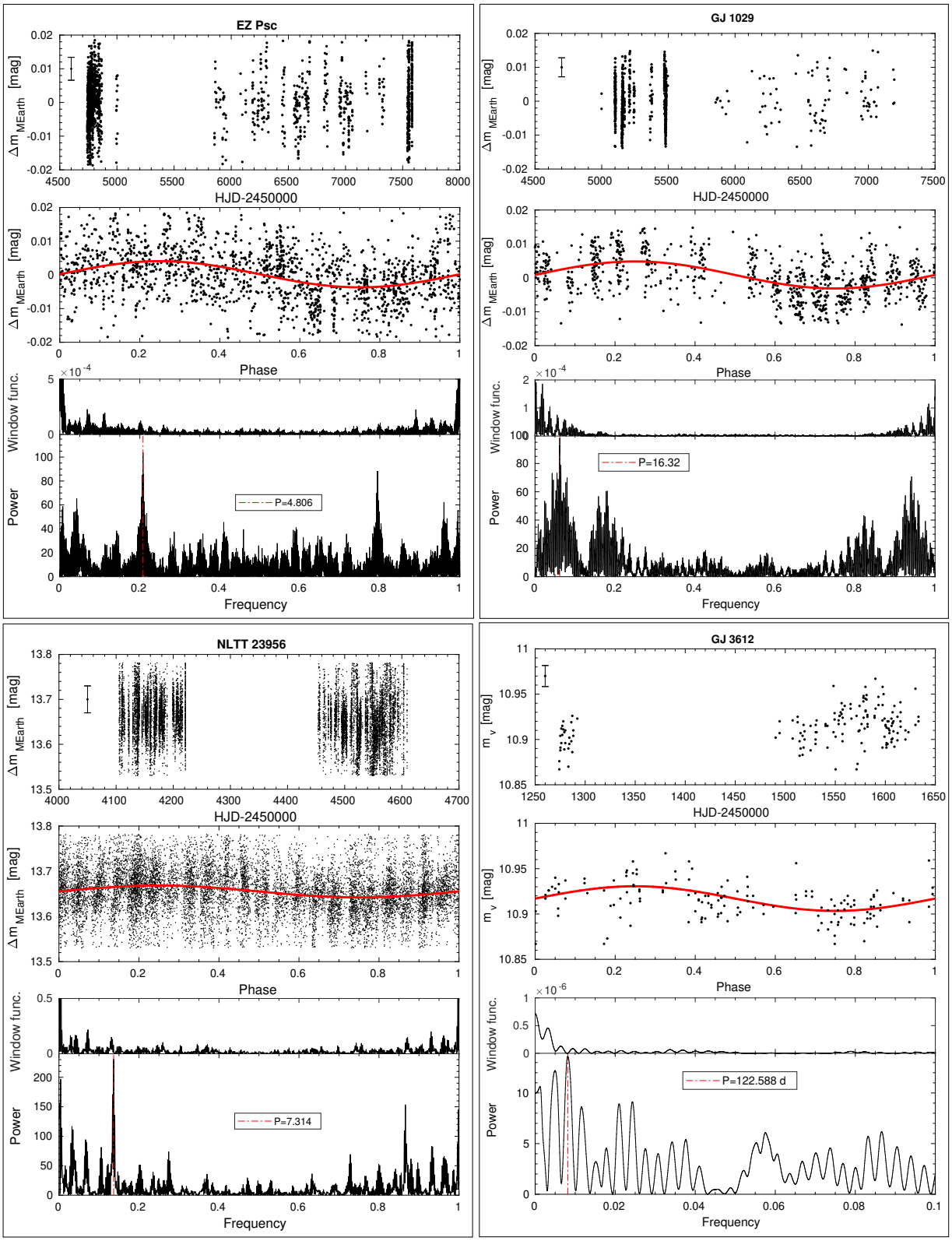

Fig. C.1. Photometry data and analysis for the stellar systems analysed in this work. Each panel corresponds to a binary system as labelled. For each system, *top panel*: light curve as a function of time and mean value of the uncertainty of the observations. *Middle panel*: light curve phase to the photometric period found and the best sinusoidal fit. *Bottom panel*: periodogram and window function of the data and the best period found (red dot-dashed line).

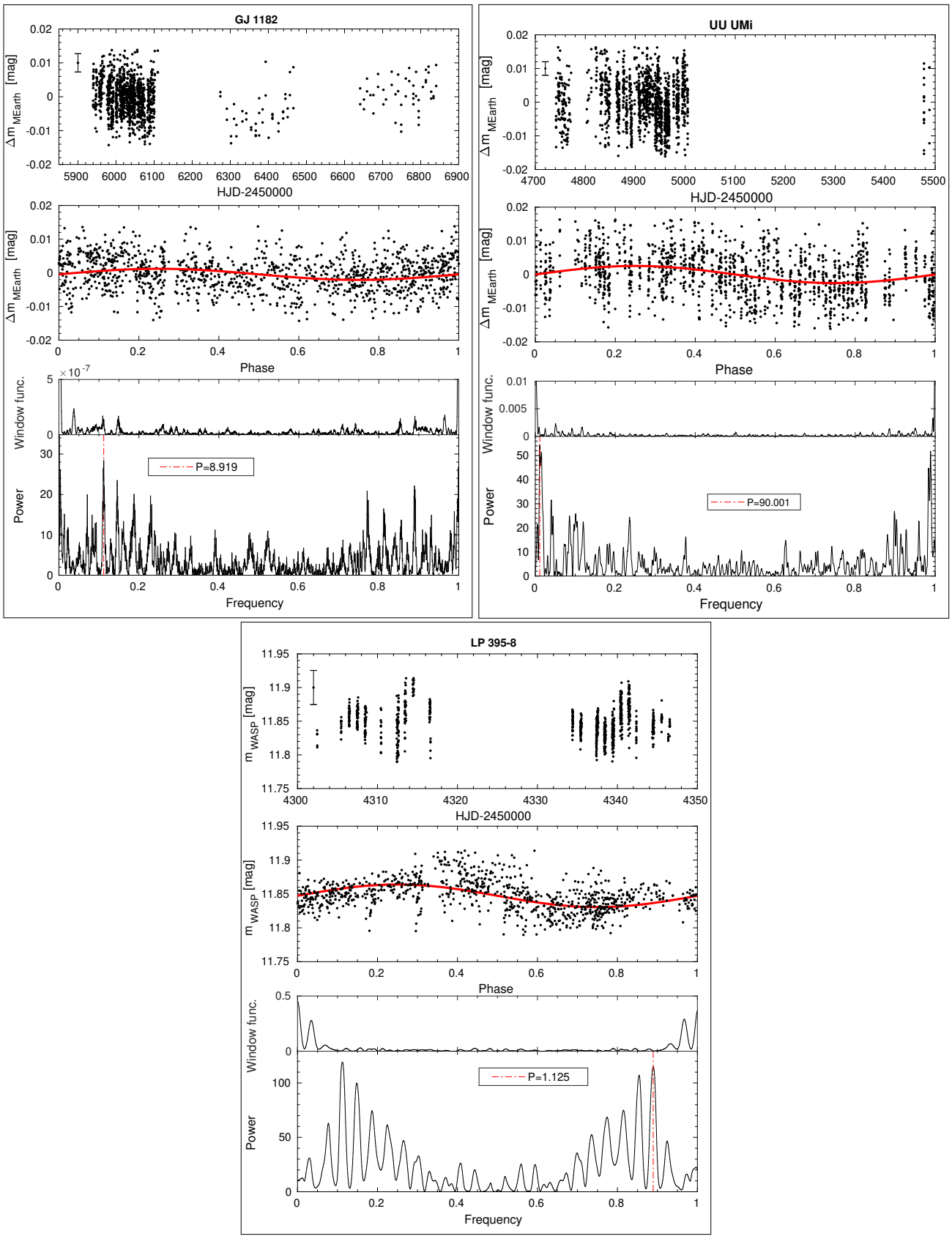

Fig. C.1. continued.

Appendix D: Known double-line spectroscopic binaries

Table D.1. Known M dwarf SB2 systems with published orbital parameters.

Name	P_{orb} (d)	T (JD-2400000)	e	ω (deg)	K_1 (km s^{-1})	K_2 (km s^{-1})	$\mathcal{M}_2/\mathcal{M}_2$	Ref.
EZ Psc	3.95652 ± 0.00008	57709.2 ± 0.2	0.0022 ± 0.0009	28 ± 20	27.64 ± 0.05	78.6 ± 0.2	0.352 ± 0.001	⋆
FF And	2.1703	42708.359	···	···	72.1	74.3	0.970	BF77
GJ 1029	95.7 ± 0.1	57857.3 ± 0.4	0.386 ± 0.005	209 ± 2	6.79 ± 0.04	9.59 ± 0.10	0.709 ± 0.009	⋆
CD-39 325[a]	0.4455960 ± 0.0000002	51868.8393 ± 0.0003	···	···	118 ± 2	163 ± 3	0.727 ± 0.019	Hel12
2MASS J02545247-0709255	11.7951 ± 0.0006	50509.94 ± 0.02	···	···	24.6 ± 0.3	43 ± 2	0.58 ± 0.02	Tor02
2MASS J03182386-0100183[a]	0.407037 ± 0.000014	53988.7993 ± 0.0006	···	···	108 ± 5	122 ± 4	0.88 ± 0.05	Bla08
2MASS J03262072+0312362[a]	1.5862046 ± 0.0000008	5478.9163 ± 0.0001	···	···	88.4 ± 0.2	94.9 ± 0.2	0.931 ± 0.002	Kra11
GJ 3236[a]	0.771260 ± 0.000002	54734.9950 ± 0.0001	···	···	86 ± 2	115 ± 2	0.746 ± 0.022	Irw09
BD+03 515	31.16 ± 0.02	47778.1 ± 0.4	0.39 ± 0.04	182 ± 5	19 ± 1	22 ± 2	0.87 ± 0.08	Tok91
2MASS J04463285+1901432[a]	0.618790 ± 0.000005	52530.2622 ± 0.0004	···	···	63 ± 1	152 ± 7	0.41 ± 0.02	Heb06
UCAC3 56-8629[a]	1.1112861 ± 0.0000004	55255.9633 ± 0.0007	0.03 ± 0.01	271.2 ± 0.2	91 ± 5	103 ± 5	0.88 ± 0.06	Lub17
DQ Tau	15.810 ± 0.006	49582.78 ± 0.23	0.58 ± 0.07	228 ± 5	22 ± 2	22 ± 2	0.96 ± 0.14	Mat97
LP 476-207	11.9623 ± 0.0005	49799.47 ± 0.04	0.323 ± 0.006	212.0 ± 0.6	9.96 ± 0.03	17.57 ± 0.03	0.567 ± 0.002	Del99
V1236 Tau[a]	2.58791 ± 0.00001	52251.512 ± 0.005	···	···	88.4 ± 0.5	95.5 ± 0.6	0.98 ± 0.02	BO06
V2212 Ori[a]	4.67390 ± 0.00006	54849.9008 ± 0.0005	0.017 ± 0.003	1.48 ± 0.01	57 ± 2	58 ± 3	0.98 ± 0.06	Gom12
2MASS J05445791-2456095[a]	4.077017 ± 0.000001	56374.0171 ± 0.0001	0.002 ± 0.002	274 ± 42	42 ± 2	58 ± 4	0.72 ± 0.06	Zho15
Ross 59	721 ± 2	58007 ± 2	0.509 ± 0.009	109 ± 2	2.91 ± 0.04	8.8 ± 0.1	0.333 ± 0.007	⋆
LHS 6100	2.63	56261.747 ± 0.006	0.010 ± 0.003	128.4 ± 35	32.29 ± 0.14	38.44 ± 0.32	0.840 ± 0.006	Ski18
QY Aur	10.428	45770.8	0.34	217.5	33.1	39.8	0.831	TP86
G 109-55	304.4 ± 0.3	48826 ± 2	0.400 ± 0.008	273.8 ± 0.9	12.47 ± 0.08	18.6 ± 0.2	0.670 ± 0.008	Del99
YY Gem[a]	0.81428	49345.112	···	···	121.2 ± 0.4	120.5 ± 0.4	0.994 ± 0.005	TR02
Ross 775[a]	1.5484492 ± 0.0000006	5473.73166 ± 0.00003	···	···	92.3 ± 0.2	99.2 ± 0.2	0.931 ± 0.003	Kra11
CU Cnc[a]	2.771472 ± 0.000004	50207.8128 ± 0.0009	···	···	68.03 ± 0.09	73.06 ± 0.09	0.931 ± 0.002	Del99
2MASS J08503296+1208239[a]	3.3439539 ± 0.0000002	57214.94178 ± 0.00003	0.014 ± 0.03	269.80 ± 0.03	48.2 ± 0.2	79.4 ± 0.9	0.607 ± 0.007	Har18
2MASS J08504984+1948364[a]	6.015742 ± 0.000002	57148.9041 ± 0.0001	0.0017 ± 0.0006	38 ± 17	34.3 ± 0.2	64.7 ± 0.7	0.531 ± 0.005	Kra17
G 41-14	7.555 ± 0.002	50471.2 ± 0.2	0.014 ± 0.002	7 ± 9	30.15 ± 0.05	36.79 ± 0.09	0.820 ± 0.002	Del99
BD-02 3000	47.709 ± 0.053	49345.44 ± 0.52	0.53 ± 0.02	81 ± 2	30.2 ± 0.6	40 ± 2	0.76 ± 0.03	Har96
NLTT 23956	5.92285 ± 0.00006	58007.4 ± 0.1	0.014 ± 0.001	289 ± 6	32.47 ± 0.06	56.15 ± 0.09	0.578 ± 0.001	⋆
2MASS J10305521+0334265[a]	1.637530 ± 0.000002	54547.83444 ± 0.00008	···	···	83.3 ± 0.2	93.6 ± 0.2	0.89 ± 0.003	Kra11
GJ 3612	119.41 ± 0.04	57718.4 ± 0.6	0.066 ± 0.002	326 ± 2	10.64 ± 0.03	21.0 ± 0.1	0.507 ± 0.003	⋆
LSPM J1112+7626[a]	41.03237 ± 0.00002	55290.0462 ± 0.0002	0.238 ± 0.006	50.1 ± 0.2	22.81 ± 0.06	32.79 ± 0.06	0.696 ± 0.002	Irw11
DP Dra	54.075 ± 0.006	50506.2 ± 0.5	0.081 ± 0.005	137 ± 3	22.0 ± 0.5	22.5 ± 0.5	0.98 ± 0.03	Del99
BD+35 2436	200.26 ± 0.09	48780.3 ± 0.4	0.53 ± 0.01	349 ± 2	17.1 ± 0.2	20.7 ± 0.4	0.83 ± 0.02	Tok97
UCAC4 847-011196[a]	0.3681414 ± 0.0000003	53473.98266 ± 0.00002	···	···	143.9 ± 0.4	156.1 ± 0.9	0.922 ± 0.006	Lop06
GJ 1182	154.2 ± 0.1	57867.82 ± 0.07	0.537 ± 0.002	275.8 ± 0.3	11.97 ± 0.03	18.00 ± 0.07	0.665 ± 0.003	⋆
HD 131976	308.884 ± 0.004	50270.22 ± 0.01	0.7559 ± 0.0002	127.56 ± 0.05	18.19 ± 0.01	27.32 ± 0.03	0.6656 ± 0.0007	For99
GU Boo[a]	0.488728 ± 0.000002	52723.9811 ± 0.0003	···	···	142.7 ± 0.7	145.1 ± 0.7	0.983 ± 0.007	Lop05
UU UMi	7927 ± 700	58118 ± 50	···	···	2.5 ± 0.2	4.5 ± 0.2	0.57 ± 0.06	⋆
G 179-55[a]	3.550018 ± 0.000002	51232.8953 ± 0.0009	···	···	56.0 ± 0.8	55.8 ± 0.8	1.00 ± 0.02	Har11
BD+11 2874	1015 ± 3	50828 ± 11	0.37 ± 0.02	340 ± 5	6.6 ± 0.3	7.0 ± 0.3	0.94 ± 0.05	Tok00
2MASS J15595050-1944373[a]	34.00070 ± 0.00009	56909.2511 ± 0.0009	0.2673 ± 0.0002	175.9 ± 0.7	28.96 ± 0.09	30.19 ± 0.09	0.959 ± 0.004	Dav16
UGCS J161630.67-251220.2[a]	2.80885 ± 0.00002	56894.7139 ± 0.0005	0.016 ± 0.009	259 ± 9	43.4 ± 0.6	47.8 ± 0.4	0.91 ± 0.01	Dav16
2MASS J16502074+4639013[a]	1.12079 ± 0.00001	53139.7495 ± 0.0008	···	···	100.5 ± 0.3	101.3 ± 0.3	0.9921 ± 0.0004	Cre05
CM Dra[a]	1.268390 ± 0.000001	46058.5640 ± 0.0003	0.005 ± 0.001	129 ± 16	72.2 ± 0.1	78.0 ± 0.1	0.93 ± 0.002	Mor09
G 203-60	3.29	5649.38 ± 0.30	0.002 ± 0.002	54 ± 33	43.87 ± 0.08	66.47 ± 0.16	0.660 ± 0.001	Ski18
GJ 644 A	626 ± 2	47185 ± 28	0.08 ± 0.02	285 ± 17	4.4 ± 0.1	2.7 ± 0.1	0.61 ± 0.08	Maz01
GJ 644 B	2.96552 ± 0.00002	47337.2 ± 0.2	0.021 ± 0.007	162 ± 21	17.2 ± 0.2	19.0 ± 0.2	0.91 ± 0.01	Maz01
BD+04 3562	34.50 ± 0.01	49178.4 ± 0.2	0.39 ± 0.02	132 ± 2	29.7 ± 0.4	35 ± 1	0.84 ± 0.03	Tok94
BY Dra	5.9751	41147.09	0.36	220	28.2	28.8	0.979	VF79
GJ 1230 A	5.06880 ± 0.00005	50643.7 ± 0.2	0.009 ± 0.001	230 ± 10	46.9 ± 0.1	49.0 ± 0.1	0.957 ± 0.003	Del99
MCC 188	10.319 ± 0.008	46188.981 ± 0.085	0.20 ± 0.01	177 ± 3	21.9 ± 0.4	23.3 ± 0.4	0.94 ± 0.02	DM88
2MASS J19324321+3636534[a]	1.6734372 ± 0.0000005	54374.8082 ± 0.0002	···	···	72 ± 2	95 ± 3	0.76 ± 0.03	Bir12
2MASS J19341550+3628271[a]	1.4985177 ± 0.0000004	54332.88980 ± 0.00008	···	···	91 ± 2	94 ± 2	0.96 ± 0.03	Bir12
2MASS J19350355+3631165[a]	2.44178 ± 0.00003	54319.83270 ± 0.00002	···	···	29.4 ± 0.5	109 ± 2	0.270 ± 0.006	Nef13
2MASS J19364065+3642460[a]	4.939095 ± 0.000002	54393.8079 ± 0.0002	···	···	55 ± 2	60 ± 1	0.92 ± 0.04	Bir12
2MASS J20115132+0337194[a]	0.6303135 ± 0.0000002	54738.74970 ± 0.00004	···	···	124.8 ± 0.1	129.9 ± 0.1	0.961 ± 0.001	Kra11
LP 395-8	1.129339 ± 0.000007	57620.08 ± 0.04	0.007 ± 0.002	352 ± 12	36.5 ± 0.1	65.3 ± 0.2	0.560 ± 0.002	⋆
GJ 810 A	812 ± 51	57822 ± 4	0.40 ± 0.05	239 ± 2	5.6 ± 0.2	6.7 ± 0.2	0.83 ± 0.04	⋆
Wolf 1084	0.795340 ± 0.000003	54140.530 ± 0.001	···	···	73.8 ± 1.4	75.4 ± 1.4	0.98 ± 0.03	Ire08
BD+40 883 A	3.2756	43270.94	0.04	3.9	39.5	57.2	0.691	Fek78
BD+40 883 B	10777.10 ± 241.06	43099 ± 17	0.72 ± 0.01	309 ± 3	3.7 ± 0.2	12 ± 2	0.32 ± 0.05	DM88
G 212-34	8.17	56488.08 ± 0.20	0.062 ± 0.012	127.8 ± 8.8	58.51 ± 0.59	64.7 ± 1.3	0.905 ± 0.016	Ski18
Ross 775	53.221 ± 0.004	48980.2 ± 0.2	0.374 ± 0.004	300 ± 1	18.7 ± 0.1	18.7 ± 0.1	1.000 ± 0.008	Del99
2MASS J21442066+4211363	3.30	56205.3381 ± 0.0057	···	···	61.16 ± 0.46	64.6 ± 2.6	0.947 ± 0.037	Ski18
CD-51 13128	1.123 ± 0.007	48467.07 ± 0.02	···	···	36 ± 2	40 ± 2	0.92 ± 0.08	JB93
FK Aqr	4.0832	37144.123	0.01	356	46.8	58.1	0.806	HM65
2MASS J23143816+0339493[a]	1.722821 ± 0.000004	54730.78778 ± 0.00004	···	···	75.4 ± 0.2	92.5 ± 0.2	0.815 ± 0.002	Kra11

Notes. Systems are sorted by their right ascension. [(a)]Eclipsing binary systems.

References. ⋆: this work; Bir12: Birkby et al. (2012); BF77: Bopp & Fekel (1977); Bla08: Blake et al. (2008); BO06: Bayless & Orosz (2006); Cre05: Creevey et al. (2005); Dav16: David et al. (2016); Del99: Delfosse et al. (1999); DM88: Duquennoy & Mayor (1988); Fek78: Fekel et al. (1978); For99: Forveille et al. (1999); Gom12: Gómez Maqueo Chew et al. (2012); Har96: Harlow (1996); Har11: Hartman et al. (2011); Har18: (Hartman et al. 2018); Heb06: Hebb et al. (2006); Hel12: Hełminiak et al. (2012); HM65: Herbig & Moorhead (1965); Ire08: Ireland et al. (2008); Irw09: Irwin et al. (2009); Irw11: Irwin et al. (2011b); JB93: Jeffries & Bromage (1993); Kra11: Kraus et al. (2011); Kra17: Kraus et al. (2017); Lop05: López-Morales & Ribas (2005); Lop06: Lopez-Morales et al. (2006); Lub17: Lubin et al. (2017); Mat97: Mathieu et al. (1997); Maz01: Mazeh et al. (2001); Mor09: Morales et al. (2009); Nef13: Nefs et al. (2013); Ski18: Skinner et al. (2018); Tok91: Tokovinin (1991); Tok94: Tokovinin (1994); Tok97: Tokovinin (1997); Tok00: Tokovinin et al. (2000); Tor02: Torres et al. (2002); TP86: Tomkin & Pettersen (1986); TR02: Torres & Ribas (2002); VF79: Vogt & Fekel (1979); Zho15: Zhou et al. (2015).